Short Telomeres and Stem Cell Exhaustion Model Duchenne Muscular Dystrophy in mdx/mTR Mice

Alessandra Sacco,[1,4,5] Foteini Mourkioti,[1,4] Rose Tran,[1] Jinkuk Choi,[2] Michael Llewellyn,[3] Peggy Kraft,[1] Marina Shkreli,[2] Scott Delp,[3] Jason H. Pomerantz,[1,6,*] Steven E. Artandi,[2] and Helen M. Blau[1,*]

[1]Baxter Laboratory for Stem Cell Biology, Department of Microbiology and Immunology, Institute for Stem Cell Biology and Regenerative Medicine
[2]Department of Medicine, Cancer Biology Program
Stanford University School of Medicine, Stanford, CA 94305, USA
[3]BioX Program, James H. Clark Center for Biomedical Engineering and Science, Stanford University, CA 94305, USA
[4]These authors contributed equally to this work
[5]Present address: Muscle Development and Regeneration Program, Sanford Children's Health Research Center, Sanford-Burnham Medical Research Institute, 10901 North Torrey Pines Road, La Jolla, CA 92037, USA
[6]Present address: Departments of Surgery and Orofacial Sciences, Division of Plastic and Reconstructive Surgery, Craniofacial and Mesenchymal Biology Program, Eli and Edythe Broad Center of Regeneration Medicine, University of California, San Francisco, San Francisco, CA 94143, USA
*Correspondence: hblau2@stanford.edu (H.M.B.), jason.pomerantz@ucsfmedctr.org (J.H.P.)
DOI 10.1016/j.cell.2010.11.039

SUMMARY

In Duchenne muscular dystrophy (DMD), *dystrophin* mutation leads to progressive lethal skeletal muscle degeneration. For unknown reasons, dystrophin deficiency does not recapitulate DMD in mice (mdx), which have mild skeletal muscle defects and potent regenerative capacity. We postulated that human DMD progression is a consequence of loss of functional muscle stem cells (MuSC), and the mild mouse mdx phenotype results from greater MuSC reserve fueled by longer telomeres. We report that mdx mice lacking the RNA component of telomerase (mdx/mTR) have shortened telomeres in muscle cells and severe muscular dystrophy that progressively worsens with age. Muscle wasting severity parallels a decline in MuSC regenerative capacity and is ameliorated histologically by transplantation of wild-type MuSC. These data show that DMD progression results, in part, from a cell-autonomous failure of MuSC to maintain the damage-repair cycle initiated by dystrophin deficiency. The essential role of MuSC function has therapeutic implications for DMD.

INTRODUCTION

Duchenne muscular dystrophy (DMD) is a devastating muscle degenerative disease caused by a mutation in dystrophin (Hoffman et al., 1987), a cytoskeletal protein that is essential for the stability of the membrane of multinucleated myofibers in skeletal muscle (Durbeej and Campbell, 2002). Absence of dystrophin results in increased fragility of the sarcolemma, leading to injury

in the presence of even mild stress (Petrof et al., 1993). DMD patients suffer from progressive loss of muscle function, leading to paralysis and death in the third decade of life (Emery, 2002). Under normal conditions, skeletal muscle is relatively quiescent when compared to high-turnover tissues such as the blood and most epithelia. However, skeletal muscle harbors considerable regenerative capacity due to the presence of adult muscle stem cells (MuSC), also known as satellite cells, which play a major role in postnatal muscle growth and repair (Collins et al., 2005; Cornelison et al., 2004; Kuang et al., 2007; Montarras et al., 2005; Sacco et al., 2008). In DMD, unrelenting, recurrent myofiber damage elicits a constant need for regeneration. Eventually, muscle tissue is supplanted by fibrosis, calcium deposits, and adipose accumulation that coincide with clinical manifestations. To date, the basis for the observed mild effects in mice and lethal effects in humans of the same genetic absence of dystrophin remain unknown. Furthermore, although clearly initiated by dystrophin deficiency, the pathophysiological cause of the failure of the repair process in muscles of DMD patients is not understood.

More than two decades ago, before the cloning of the DMD gene, we obtained data that suggested that muscle cells in DMD patients have diminished regenerative capacity as a consequence of replicative aging (Blau et al., 1983; Webster and Blau, 1990). Human DMD myoblasts exhibited a severe proliferation deficit in vitro that became more pronounced with patient age, resulting in a yield of myoblasts per gram muscle of 5% of normal, and the proliferative potential of the remaining myoblasts was severely impaired. However, this proliferative defect did not segregate with the X chromosome in studies of myoblast clones from doubly heterozygous carriers for two X-linked loci, DMD and a Mediterranean histologically detectable heat-labile variant of G6PD, and was therefore dependent on additional factors (Webster et al., 1986).

Recent studies support and extend the early findings that myoblasts from DMD have impaired replicative potential and suggest that telomere shortening is a common feature of dystrophic human muscle cells with increasing age. This correlates with their limited ability to regenerate DMD tissues upon transplant (Mouly et al., 2005). Indeed, a 14-fold greater shortening of telomeres in DMD patients relative to healthy individuals has been reported (Decary et al., 2000). Telomeres are DNA repeats that protect chromosome ends from illicit recombination, fusion, and degradation leading to genomic instability (Palm and de Lange, 2008). Telomere length is maintained by the enzyme telomerase, which adds telomere repeats to chromosome ends, ensuring their proper replication (Greider and Blackburn, 1985). Cell proliferation in settings of insufficient telomerase results in progressive telomere shortening, ultimately leading to replicative senescence as chromosome end protection is compromised at a subset of short telomeres (Rodier et al., 2005; Sherr and DePinho, 2000). Telomere shortening also accompanies aging of mitotically active human tissues with high turnover, including blood, liver, skin, testis, and kidneys (Aikata et al., 2000; Friedrich et al., 2000; Lindsey et al., 1991; Takubo et al., 2000; Vaziri et al., 1993). In contrast, analysis of telomeres in skeletal muscle during aging in whole-tissue assays reveals only a mild shortening (Decary et al., 1997; Renault et al., 2002), presumably reflecting the low rate of proliferation of myogenic progenitors and muscle tissue turnover during normal aging. In agreement with these findings, studies of telomerase knockout mice revealed short dysfunctional telomeres that profoundly impaired progenitor cell function in actively renewing tissues. This led to atrophy and reduced regenerative potential, whereas more quiescent low-turnover tissues such as muscle were unaffected (Allsopp et al., 2003; Lee et al., 1998; Rudolph et al., 1999).

A major challenge hindering the development of effective therapies for DMD has been the lack of an animal model that closely recapitulates the disease progression in humans. The most widely used animal model for DMD, the mdx mouse, exhibits only a mild dystrophic phenotype, although like DMD patients, it lacks functional dystrophin due to a point mutation in the dystrophin gene (Bulfield et al., 1984; Hoffman et al., 1987; Ryder-Cook et al., 1988). Muscles of mdx mice, like those in DMD patients, undergo repeated cycles of degeneration and regeneration, but for unknown reasons, the mice exhibit only transient muscle weakness and never exhibit the profound loss of muscle strength and death observed in DMD patients (DiMario et al., 1991; Straub et al., 1997). Here, we test the hypothesis that species-specific differences in telomere length account for the differential proliferative capacity of muscle cells derived from DMD patients and mdx mice and consequent disparate disease progression between the two species. Humans have relatively short telomeres of ~5–15 kilobases in comparison to in-bred strains of laboratory mice, which have telomeres that are typically > 40 kilobases (Kipling and Cooke, 1990). This greater telomere reserve could endow MuSC in mice with a prolonged regenerative capacity and mild muscle phenotype despite dystrophin deficiency. In support of this hypothesis, lack of a disease phenotype in mouse models of other human diseases, such as Werner and ataxia-telangiectasia syndromes, has been linked to species-specific differences in telomere length, as when these

models were crossed with mice lacking telomerase activity, the disease became apparent (Chang et al., 2004; Wong et al., 2003).

Here, we generate mdx mice lacking telomerase activity and show that dystrophin deficiency coupled with telomere dysfunction recapitulates the severe phenotypic characteristics of muscular dystrophy in humans, including profound loss of muscle force, poor performance on a treadmill, increased serum creatine kinase (CK) levels, accumulation of fibrosis and calcium deposits within skeletal muscle tissues, kyphosis, and shortened life span. We show that the severity of the disease progressively worsens with age. Moreover, MuSC exhibit a severe proliferation deficit both in vitro and in vivo, inability to respond to tissue injury, and markedly reduced engraftment and contribution to muscle repair. Transplantation of WT MuSC into mdx mice lacking telomerase activity ameliorates the dystrophic phenotype histologically. Together, these results indicate that the combination of the structural defect of dystrophin deficiency that leads to muscle degeneration together with the progressive exhaustion of functional MuSC generates the dystrophic phenotype. These findings support the hypothesis that, in humans, DMD is initiated by the genetic defect but, as suggested by our earlier findings (Blau et al., 1983; Webster et al., 1986), develops progressively into an exhaustion of cells with regenerative potential.

RESULTS

We generated dystrophic mice lacking telomerase activity by crossing C57Bl6 mdx female mice homozygous for the dystrophin mutation (Im et al., 1996) with C57Bl6 mice heterozygous for the telomerase RNA component Terc (mTR) (Blasco et al., 1997) (Figure 1A). The resulting mdx/mTR^{Het} mice were further crossed to generate double-mutant mdx mice totally lacking dystrophin and telomerase activity (designated herein as first-generation mdx/mTR^{G1}). The mdx/mTR^{G1} mice were, in turn, intercrossed to produce second-generation mdx/mTR^{G2} mice. This strategy yields the same strain of dystrophic mice that lack telomerase, which is critical, as telomere length differs among mouse strains (Hemann et al., 2001). In addition, the dystrophic phenotype is analyzed in mice with different telomere lengths, as shortening increases in mTR mice with successive generations.

Severe Muscular Dystrophy in mdx/mTR^{G2} Mice

To assess the severity of muscular dystrophy, we carried out three essential controls. We compared mdx/mTR^{G1} and mdx/mTR^{G2} mice with mdx/mTR^{Het} mice, as these mice lack dystrophin and one copy of the Terc gene, providing the most stringent same-strain control. As a second control, we analyzed mTR^{G2} mice, which are generation matched for telomerase deficiency but have wild-type dystrophin, which was essential in order to rule out the possibility that a phenotype resulted from telomerase deficiency alone. Finally, our studies were restricted to male mice, as the disease is X-linked and differences in sex can confound results.

We first tested serum creatine kinase (CK) levels, an established indicator of skeletal muscle damage in mice that is a diagnostic indicator of DMD. Eight-week-old mdx/mTR^{G2} males
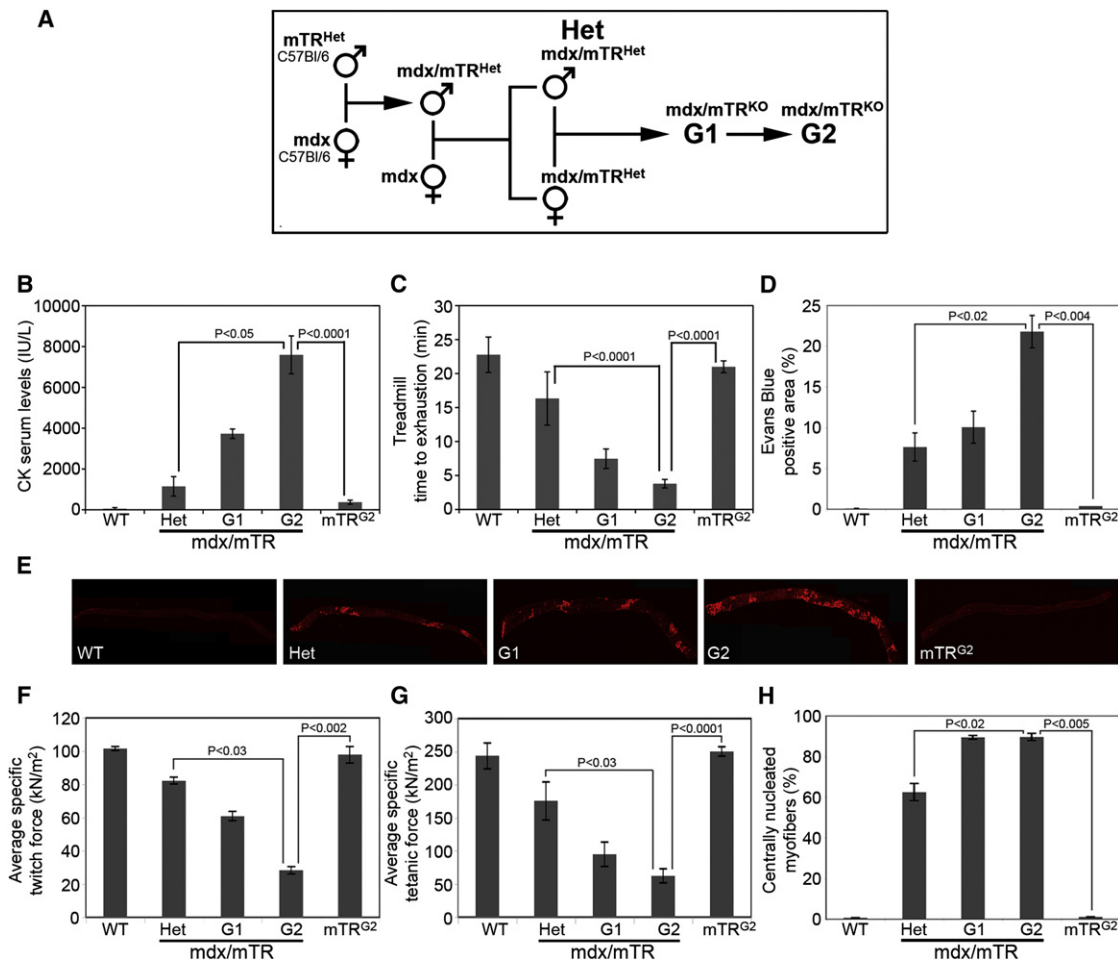
Figure 1. Evidence of Severe Muscular Dystrophy in mdx/mTR^{G2} Mice

(A) Scheme of mouse breeding.

(B) Serum CK levels in 8-week-old males. A marked increase in CK levels is seen in mdx/mTR^{G2} animals. Data are represented as average ± SEM. n ≥ 10; p values are indicated in the graph. See also Figure S1A.

(C) Eight-week-old males were subjected to the treadmill test, and their performance was measured as time to exhaustion. mdx/mTR^{G2} animals were severely impaired in their muscle endurance, compared to WT or mdx/mTR^{Het}. Data are represented as average ± SEM. n ≥ 5; p values are indicated in the graph. See also Figures S1B and S1C.

(D) Quantification of Evans blue dye uptake in diaphragm muscle of 8-week-old nonexercised mice (% EBD$^+$ area). Data are represented as average ± SEM. n = 3; p values are indicated in the graph. See also Figure S2.

(E) Representative images of Evans blue dye uptake in diaphragm muscles from the various genotypes.

(F and G) Muscle force was measured in the lateral gastrocnemius muscle in vivo in 8-week-old anesthetized animals by electrical stimulation of the sciatic nerve and was expressed relative to cross-sectional area (P$_0$/CSA, force per square meter, kN/m^2). Data are represented as average ± SEM. n ≥ 4; p values are indicated in the graph. See also Figure S1D.

(H) Quantification of centrally nucleated myofibers in gastrocnemius muscles of 8-week-old mice from the indicated genotypes. Data are represented as average ± SEM. n = 3; p values are indicated in the graph.

already have remarkably elevated serum CK (7594 ± 928 IU/l), compared to mdx/mTR^{Het} males (1148 ± 477 IU/l) (Figure 1B), approximating human DMD levels (6000–8000 IU/l in 10-year-old patients) (Zatz et al., 1991). However, by 60 weeks of age, CK levels decline in mdx/mTR^{G2} mice (Figure S1A available online), consistent with CK levels in DMD patients that peak at 1–6 years of age when active muscle degeneration is occurring and then decrease with age as muscle tissue is progressively lost (Zatz et al., 1991). Heterozygous mdx/mTR^{Het} mice with increased age show increased CK levels, presumably due to

slower progression of the disease (Figure S1A). Serum CK levels are indistinguishable for mTR^{G2} and healthy WT mice (Figure 1B, p > 0.05), consistent with previous studies showing that telomere deficiency preferentially affects highly proliferative organs, but not skeletal muscle (Allsopp et al., 2003; Artandi, 2006; Herrera et al., 1999; Lee et al., 1998). The progressive elevation of CK seen in mdx/mTR^{G1} and mdx/mTR^{G2} animals suggests that muscle damage increased with successive generations, implicating telomere attrition as a cooperating factor with dystrophin deficiency in disease manifestation.
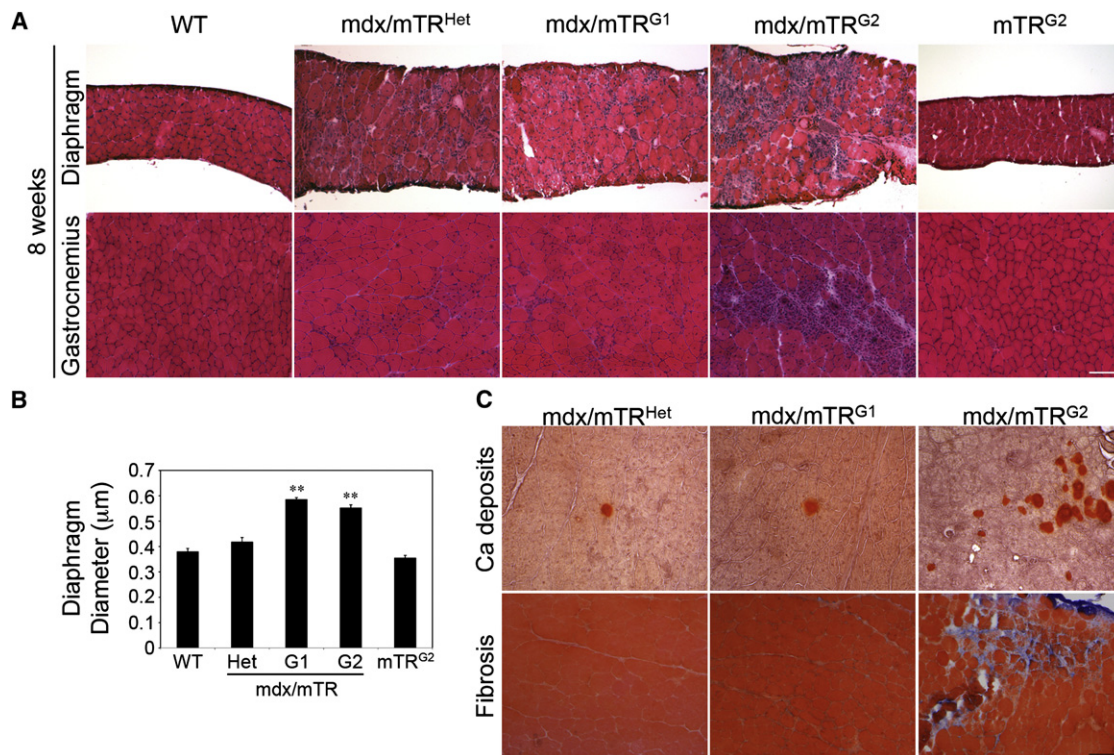
Figure 2. Histological Evidence of Severe Muscular Dystrophy in Muscles from mdx/mTR^G2 Mice

(A) Hematoxylin and eosin staining of transverse sections of diaphragm (top) and gastrocnemius (bottom) muscles from the indicated genotypes at 8 weeks of age. Scale bar, 120 μm. See also Figure S2.

(B) Average diaphragm diameter is significantly increased in 8-week-old mdx/mTR^KO mice. Data are represented as average ± SEM. n = 3; p < 0.05.
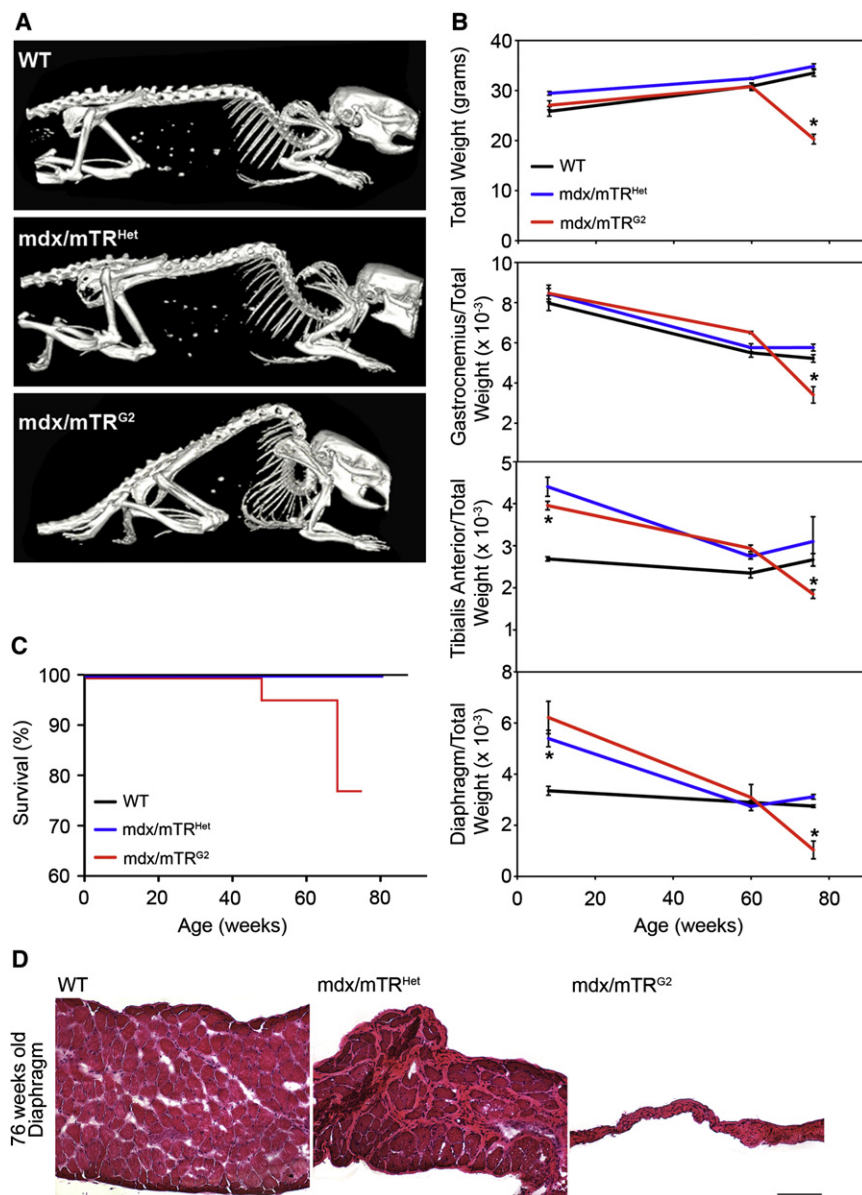
(C) Alizarin red staining to visualize calcium deposits (top) and Gomori staining for collagen deposition (bottom) in muscle transverse sections from 8-week-old mice. Scale bar, 120 μm.

Skeletal muscle damage is also evident as myofiber membrane permeability, measured by Evans blue dye (EBD) uptake (Straub et al., 1997). Diaphragm and gastrocnemius muscles of 8-week-old mdx/mTR^G2 male mice exhibit a significant increase in the percentage of EBD-positive areas, compared to mdx/mTR^Het or mdx/mTR^G1 mice (Figures 1D and 1E and Figure S2). Control mTR^G2 mice are indistinguishable from WT mice, confirming that the absence of telomerase activity per se is not sufficient to trigger skeletal muscle damage. Membrane permeability significantly worsens with age, as 60-week-old mdx/mTR^G2 animals exhibit higher EBD incorporation (Figure S2). Together, these data indicate that, in the absence of telomerase, dystrophin deficiency causes progressive skeletal muscle damage in mice.

To assess muscle performance, we first analyzed time to exhaustion on a treadmill. Eight-week-old mdx/mTR^G2 mice run for a significantly shorter time than control WT (3.8 ± 0.6 versus 22.8 ± 2.6 min) or mdx/mTR^Het mice (16.3 ± 3.9 min). Muscle performance further worsens with age, as 24-week-old mdx/mTR^G2 mice barely run at all (1.1 ± 0.6 min) (Figure 1C and Figure S1B). By contrast, age-matched mTR^G2 mice are indistinguishable from WT mice at both 8 and 24 weeks of age (Figure 1C and Figure S1B). A second well-established assay of muscle performance is the grid test, a measure of the length of time that mice can support their weight by holding onto a rod. The results of the grid test in 8-week-old mice paralleled the treadmill experiment, as mdx/mTR^G2 mice are able to hold onto the grid for a substantially shorter time than controls (Figure S1C). Third, we measured specific muscle force of gastrocnemius muscles. To avoid potential artifacts due to muscle excision, we assayed force generation in vivo in intact muscles in 8-week-old anesthetized animals (Blaauw et al., 2008). Lateral gastrocnemius muscle twitch force, tetanic force, and tetanic tension are markedly decreased in mdx/mTR^G1 and further decrease in mdx/mTR^G2 mice, compared to control WT, mdx/mTR^Het, and mTR^G2 mice (Figures 1F and 1G and Figure S1D), providing direct evidence for progressively severe muscle weakness.

Histologically, the percentage of centrally nucleated myofibers, a hallmark of muscle regeneration, is increased in mdx/mTR^Het mice (63% ± 4%) relative to WT (0.7% ± 0.1%) but is further increased in mdx/mTR^G1 and mdx/mTR^G2 muscles (90% ± 1%) (Figure 1H and Figure 2A), providing evidence of a marked increase in tissue damage and regenerative activity in most fibers at 8 weeks of age. Further histological analyses of diaphragm and gastrocnemius muscles from 8-week-old mdx/mTR^G2 mice reveal a marked increase in myofiber diameter heterogeneity, mononuclear cellular infiltration, necrosis, and

Muscular Dystrophy in mdx/mTR^{G2} Mice Progresses with Age

The severe progression of DMD associated with age is not recapitulated in mdx mice. Kyphosis of the spine is a classical clinical manifestation of DMD due to uneven weakening of trunk muscles and substitution with connective tissue and fat (Oda et al., 1993; Wilkins and Gibson, 1976). SPECT-CT imaging revealed that kyphosis in a cohort of aging mice is substantially more pronounced in mdx/mTR^{G2} mice than in age-matched mdx/mTR^{Het} controls at 76 weeks of age (Figure 3A).

We analyzed the severity of muscle wasting by assessing a loss of both total body weight and specific muscle weight due to atrophy, which is typically exacerbated with increasing age in DMD patients. Total body weight is disproportionately reduced in mdx/mTR^{G2} mice compared to controls at 76 weeks of age (Figure 3B). When controlled for total body weight, all genotypes exhibit a progressive decrease in muscle weight with age, but the drop is accelerated in mdx/mTR^{G2} muscles after 60 weeks. In 8-week-old mice, the diaphragm and tibialis anterior mdx/mTR^{G2} muscles exhibit an increase in weight relative to total body weight (Figure 3B), consistent with observations in DMD patients, whose body weight transiently increases at young ages but then decreases at later ages due to skeletal muscle atrophy (McDonald et al., 1995). The weight of control testis tissue, a high proliferative organ, does not change significantly among genotypes, indicating that the tissue atrophy is specific to muscles (Figure S5). Kaplan-Meyer survival analyses show that mdx/mTR^{G2} mice have reduced life span, starting to die at 48 weeks of age, whereas mdx/mTR^{Het} do not

overall altered tissue structure relative to age-matched controls (Figure 2A). Importantly, muscle histology from mTR^{G2} control mice is indistinguishable from WT mice. Diaphragm diameter of mdx/mTR^{Het} is increased compared to WT, consistent with ongoing tissue damage and repair (Figures 2A and 2B) and further increases in mdx/mTR^{G1} and mdx/mTR^{G2} mice, due primarily to massive cellular infiltration (Figures 2A and 2B). Aggregates of calcium deposition and fibrotic regions are substantially increased in mdx/mTR^{G2} muscle (Figure 2C), by contrast with mdx/mTR^{Het} and mdx/mTR^{G1} muscles. Thus, although the control mdx/mTR^{Het} mice undergo substantial muscle regeneration, as indicated by the relatively high frequency of centrally nucleated myofibers, the tissue histology is not compromised compared with mdx mice lacking telomerase activity (G1 and G2).
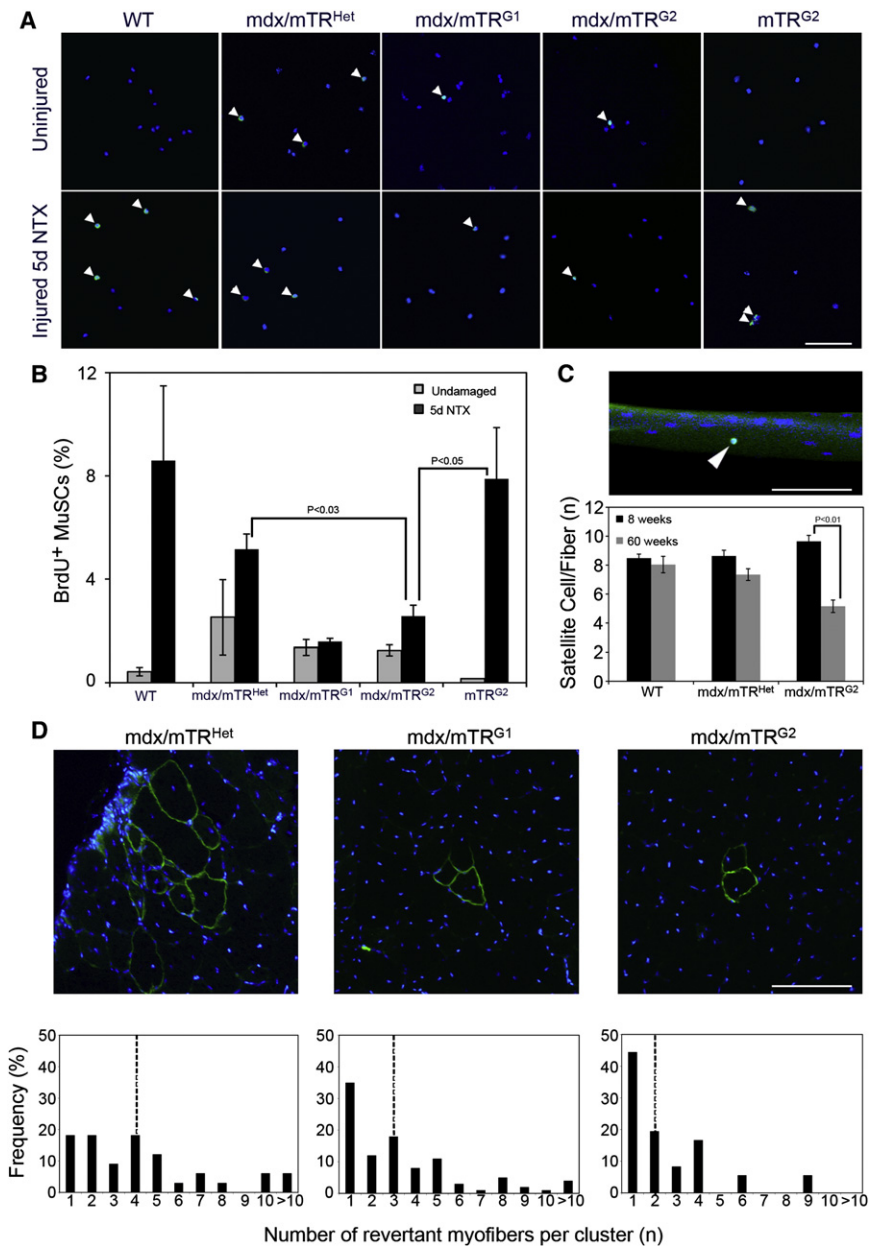
Figure 4. Muscle Stem Cells from mdx/mTR^{G2} Mice Exhibit Impaired Proliferation In Vivo

(A) Eight-week-old undamaged or NTX-damaged mice were pulsed with BrdU for 24 hr prior to tissue harvesting. MuSC were isolated by FACS, and immunofluorescence for BrdU (green) and Hoechst (blue) was performed. Representative images of MuSC from all genotypes are shown. Arrowheads indicate BrdU$^+$ cells. Scale bar, 80 μm. See also Figure S4.

(B) Percentage of BrdU$^+$ MuSC represented as average ± SEM. n ≥ 3; p values are indicated in the graph.

(C) Single fibers were isolated from tibialis anterior muscles at the indicated ages and stained for Pax7 (green) and nuclei (blue). Representative image showing a single fiber with a Pax7$^+$ satellite cell (arrowhead). Scale bar, 50 μm (top). Graph showing number of Pax7$^+$ satellite cells/fiber. n = 3 animals/group and 50–100 myofibers/animal. Data are represented as average ± SEM (bottom).

(D) Representative images of transverse sections of gastrocnemius muscles from the indicated genotypes at 8 weeks of age immunostained for dystrophin (green) and nuclei (blue). Scale bar, 100 μm (top). Graphs showing distribution of size of revertant myofiber clusters (dotted lines in the graphs represent the median of cluster size) (bottom).

show a difference compared to WT animals (Figure 3C). Finally, histological analyses of limb muscles from 76-week-old animals reveal pronounced tissue damage in mdx/mTR^{G2} mice, with extensive fibrosis and immune cell infiltration (Figure S3). Most notably, diaphragm muscles from mdx/mTR^{G2} mice at 76 weeks of age have atrophied to a small remnant of their original size, suggesting that respiratory failure is the cause of premature death (Figure 3D).

Impaired Proliferation of mdx/mTR^{G2} MuSC in Mice In Vivo

We hypothesized that the severe muscle phenotype observed in mdx/mTR^{G2} animals is caused by defects in MuSC function. To test this possibility, we assessed MuSC proliferation in vivo by assaying undamaged or acutely notexin injured tibialis anterior muscles (Harris and MacDonell, 1981) injected intraperitoneally with bromo-deoxyuridine (BrdU) 24 hr prior to harvesting. MuSC were then isolated by FACS to > 90% purity for all genotypes (Figure S4), as previously described (Sacco et al., 2008), and analyzed for BrdU incorporation. In WT mice in undamaged conditions, only 0.4% ± 0.2% of MuSC were BrdU$^+$ (Figures 4A and 4B), consistent with previous reports that adult MuSC are largely quiescent in steady-state conditions (Cerletti et al., 2008). However, upon notexin injury, WT MuSC are activated and enter the cell cycle, and 8.6% ± 2.9% are BrdU$^+$ (Figures 4A and 4B). In undamaged mdx/mTR^{Het} mice, 2.5% ± 1.4% of MuSC are BrdU$^+$, which is higher than WT mice, consistent with ongoing tissue regeneration due to dystrophin deficiency. MuSC from mdx mice are able to respond appropriately to acute injury by entering the cell cycle (5.1% ± 0.6%). In contrast, MuSC from mdx/mTR^{G1} (1.4% ± 0.3%) and mdx/mTR^{G2} (1.3% ± 0.2%) mice exhibit markedly reduced BrdU incorporation in the absence of notexin damage (Figures 4A and 4B), which does not significantly increase upon injury in mdx/mTR^{G1} (1.6% ± 0.1%) and mdx/mTR^{G2} mice (2.5% ± 0.4%), indicating a severe defect in MuSC proliferation in response to tissue damage.
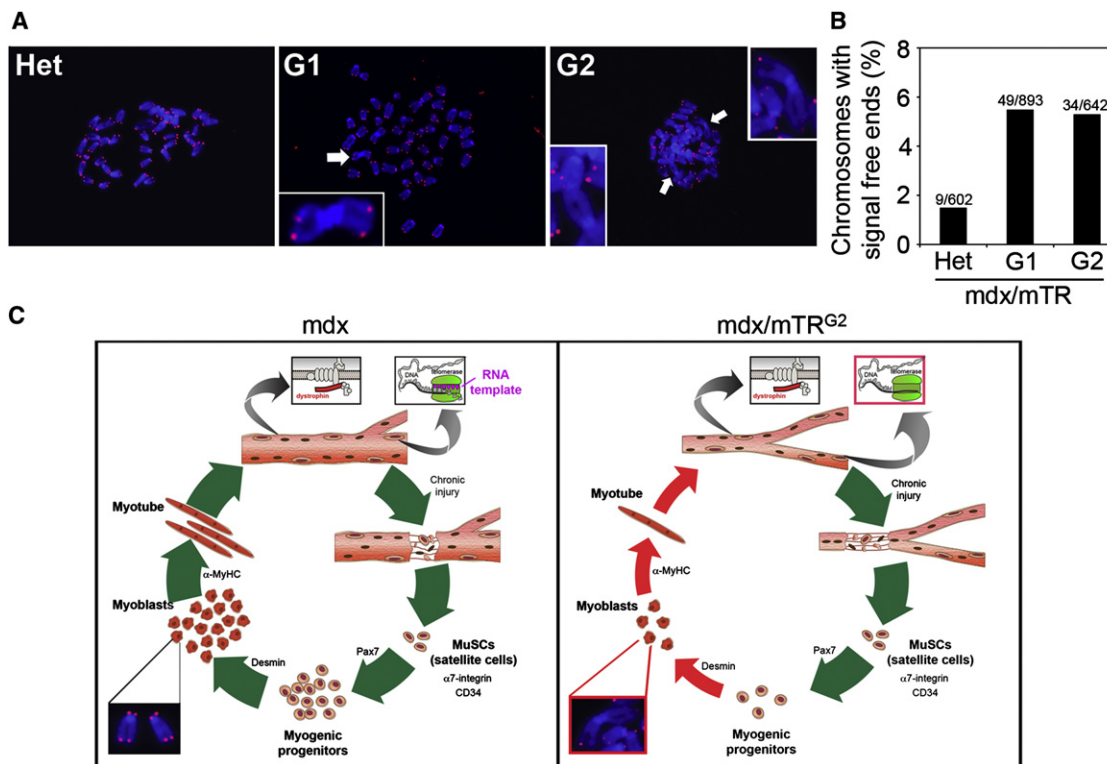
Figure 5. Telomere FISH Analysis in Primary Myoblasts

(A) Representative images of FISH on metaphase spreads from mdx/mTR[Het], mdx/mTR[G1], and mdx/mTR[G2] (red, telomeres; blue, Hoechst). Arrows show end-to-end fusion of chromosomes, indicating genomic instability.

(B) Graph showing the quantification of percentage of chromosomes with signal-free ends (total number of chromosomes analyzed are shown on top of each bar). p < 0.03. See also Figure S5.

(C) Scheme representing the series of events during muscle regeneration in the mdx mouse model (left) compared to the mdx/mTR[G2] dystrophic model (right). Critical telomere shortening and chromosomal fusions in mdx/mTR[G2] muscle cells result in impaired ability to sustain tissue regeneration.

Of note, proliferative MuSC behavior from control mTR[G2] mice is not impaired and is indistinguishable from WT mice. These data highlight that MuSC become severely impaired when the absence of dystrophin is combined with the absence of telomerase activity.

The number of Pax7^{+} satellite cells per myofiber (8.7 ± 0.6 in WT, 7.7 ± 0.1 in mdx/mTR[Het], and 8.5 ± 0.8 in mdx/mTR[G2]) is not statistically different among the different genotypes (p > 0.05) (Figure 4C), demonstrating that the observed decline in BrdU[+] MuSC is not the result of reduced numbers of satellite cells but, rather, a functional defect at this age. However, in older mice (60 weeks), the number of satellite cells is markedly reduced in aged mdx/mTR[G2] mice (Figure 4C), mirroring the severity of disease progression.

Another measure of MuSC proliferative potential in vivo is an analysis of clusters of revertant myofibers. Revertant myofibers express dystrophin protein due to a compensatory mutation in somatic cells (Hoffman et al., 1990). If the mutation takes place in a MuSC, upon proliferation, this MuSC will participate in the regeneration of myofibers in its close proximity, giving rise to a cluster of dystrophin[+] myofibers. We observe a progressive reduction in revertant myofiber cluster size in successive mdx/mTR generations, with the median cluster size in mdx/mTR[Het],

mdx/mTR[G1], and mdx/mTR[G2] declining progressively (Figure 4D), consistent with a progressive reduction in MuSC proliferative potential.

Critically Shortened Telomeres in Myoblasts from mdx/mTR[G1] and mdx/mTR[G2] Mice

Telomeres were analyzed by hybridization of a telomere-specific probe to metaphase chromosomes by fluorescence in situ hybridization (telomere FISH). This assay requires large numbers of mitotic cells in metaphase. Because methods for cultivating MuSC in sufficient numbers do not yet exist, we analyzed the derivatives of MuSC, myoblasts, isolated as previously described (Rando and Blau, 1994). Chromosome ends lacking detectable telomere repeats (signal-free ends [SFEs]) are detected at an increased frequency of 49/893 (5.5%) in mdx/mTR[G1] and 34/642 (5.3%) in mdx/mTR[G2] mice versus 9/602 (1.5%) in mdx/mTR[Het] mice (Figures 5A and 5B). The 5% frequency of SFE seen in mdx/mTR[G1] and mdx/mTR[G2] mice is not detected even in highly proliferative organs until later generations in mice lacking Terc (Blasco et al., 1997), providing evidence that this increased frequency is not due to Terc absence alone. In addition, in metaphase spreads of myoblasts from mdx/mTR[G1] and mdx/mTR[G2] mice, end-to-end chromosome

A

mdx/mTR^Het   mdx/mTR^G2

B

C

D

E

F
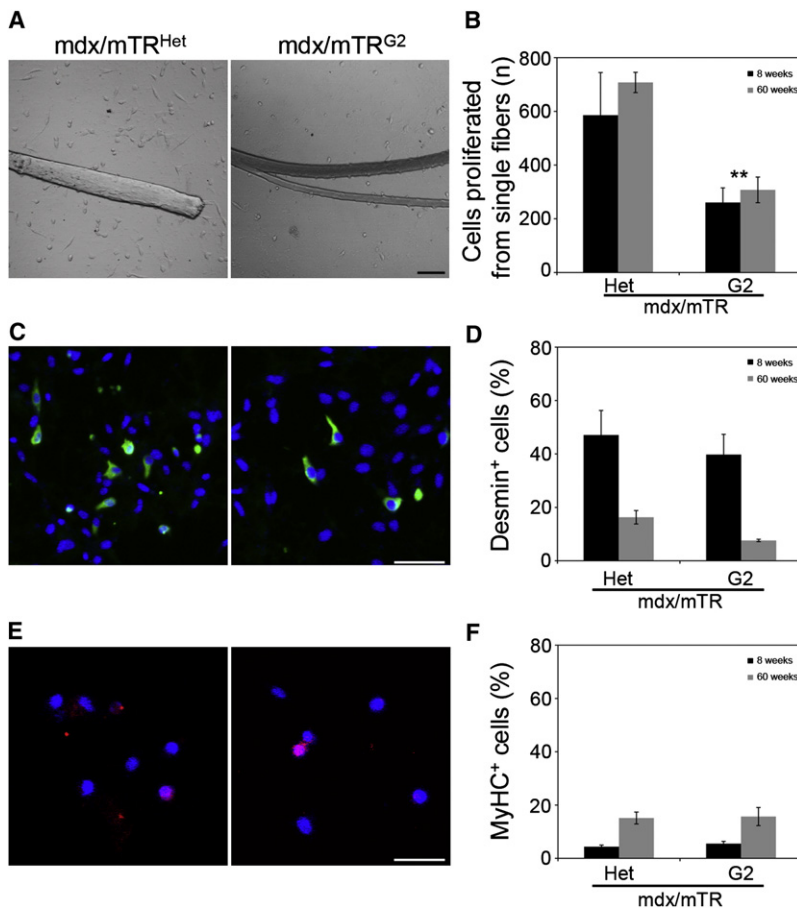
Figure 6. Muscle Stem Cells from mdx/mTR^G2 Mice Exhibit Impaired Proliferation In Vitro

(A) Single myofibers were isolated from 8- and 60-week-old animals and cultured for 96 hr. Representative images of cultures show a proliferation defect in mdx/mTR^G2 muscles, compared to mdx/mTR^Het muscles. Scale bar, 50 μm. See also Figure S6.

(B) Graph showing quantification of proliferation capacity as total number of cells derived per myofiber at 96 hr. Data are represented as average ± SEM. n = 3; p < 0.05.

(C) Representative images of immunofluorescence staining of fiber cultures for desmin (green) and nuclei by Hoechst 33258 (blue). Scale bar, 50 μm.

(D) Graph showing quantification of percentage of desmin$^+$ cells in cultures derived from single myofibers. Data are represented as average ± SEM. n = 3; p > 0.05.

(E) Representative images of immunofluorescence staining of fiber cultures for myosin heavy chain (red) and nuclei by Hoechst 33258 (blue). Scale bar, 50 μm.

(F) Graph showing quantification of percentage of MyHC$^+$ cells in cultures derived from single myofibers. Data are represented as average ± SEM. n = 3; p > 0.05.

8-week-old animals, and the proliferative potential of MuSC crawling off myofibers was analyzed after 4 days of culture. Satellite cells derived from mdx/mTR^G2 myofibers exhibit reduced proliferative potential (261 ± 54 cells/fiber) compared to mdx/mTR^Het myofibers (586 ± 157 cells/fiber) (Figures 6A and 6B). As described above (Figure 4C), the number of satellite cells per myofiber is not altered at this age, indicating that the observed differences in cell number result from a cell-autonomous proliferative defect in MuSC from mdx/mTR^G2 mice caused by dysfunctional telomeres. The reduction in satellite cell proliferation persists with age; at 60 weeks, satellite cells from mdx/mTR^G2 mice give rise only to 40% as many cells (307 ± 47) as controls (707 ± 37) (Figure 6B).

To assess whether a reduction in the proliferation capacity is followed by a change in the differentiation efficiency, staining for desmin and myosin heavy chain, two established myogenic markers, was performed in vitro. The percentage of desmin$^+$ cells is not significantly different between mdx/mTR^Het (47% ± 8%) and mdx/mTR^G2 myofibers (40% ± 21%), indicating that there is no impairment in mdx/mTR^G2 satellite cells to transition to myoblasts (Figures 6C and 6D). Of note, with age, the myogenic potential (desmin expression) is substantially reduced in both genotypes (Figure 6D), consistent with previous studies reporting a decreased myogenic potential in muscle cells from dystrophic and aged mice (Bockhold et al., 1998; Brack et al., 2007). Myosin heavy-chain expression shows that spontaneous terminal differentiation does not differ significantly between mdx/mTR^Het and mdx/mTR^G2 cells in young or old mice (Figures 6E and 6F). These data confirm that satellite cell differentiation properties do not differ, whereas the proliferative function does. With increased age, the absolute number of MuSC declines (Figure 4C), compounding the proliferative defect and leading to an even more pronounced deficit in cells available for muscle repair.

fusions were detected (Figure 5A, arrows), indicating that the telomere shortening in these cells leads to genomic instability. In marked contrast, in 602 chromosomes analyzed from mdx/mTR^Het myoblast metaphase spreads, no end-to-end fusions were detected. SFEs represent chromosome ends with the shortest telomeres and correlate with an increased incidence of chromosome fusions and tissue dysfunction in vivo in telomerase knockout mice (Chang et al., 2004). This result strongly supports our hypothesis that exhaustion of proliferative potential in dystrophic MuSC, via telomere dysfunction, is the direct cause of muscular dystrophy progression.

Analyses of spleen and testis reveal that these two high-proliferative organs are not affected in the generations analyzed (Figure S5), which argues against the possibility that the effects observed are due to the absence of Terc alone and in favor of a muscle-specific etiology. A scheme depicts the effects of Terc loss in the etiology of DMD (Figure 5C).

Impaired Proliferation Potential of MuSC from mdx/mTR^G2 mice in Culture

To further test whether the cell-autonomous changes in muscle tissue were caused by reduced proliferative potential of MuSC in mdx/mTR^G2 mice, we assessed their behavior in vitro. Single myofibers were isolated from tibialis anterior muscles from

mdx/mTR^G2 MuSC Are Impaired in Engrafting upon Transplantation

To test the combined effects of mdx mutation and telomere dysfunction on MuSC function in vivo, we assessed the ability of purified MuSC to engraft and proliferate upon transplantation into recipient muscles. Freshly isolated MuSC (Sacco et al., 2008) were infected with a lentivirus expressing GFP, and 3000 cells were transplanted into irradiated tibialis anterior muscles of immunodeficient NOD/SCID mice (Figure 7A). The infection efficiency approximated 90% and was not statistically different among samples (Figure 7B, p > 0.05). Three weeks posttransplantation, mdx/mTR^Het MuSC contributed to an average of 200 ± 30 GFP^+ myofibers (Figure 7C). Conversely, MuSC isolated from mdx/mTR^G2 mice were significantly impaired in their engraftment capacity, contributing to substantially lower numbers of myofibers, 81 ± 22 (Figure 7C). These data corroborate our in vitro analyses and show that MuSC from mdx/mTR^G2 mice have a cell-autonomous defect in proliferation that compromises their ability to generate new muscle fibers in vivo.

To investigate a potential effect of telomere erosion on myofiber degeneration, we induced acute injury by injection of notexin in 8-week-old animals and performed histological analyses at day 3 after injury. The extent of muscle damage was comparable between mdx/mTR^Het and mdx/mTR^G2, indicating that mdx/mTR^G2 mice are not more sensitive to this type of tissue injury (Figure S6). In addition, the infiltrate of hematopoietic (CD45^+ cells), macrophages (CD11b), and lymphocytes (B220) is equally represented in mdx/mTR^Het and mdx/mTR^G2 (Figure S6). These results indicate that mdx/mTR^G2 mice are competent to mount an inflammatory response to tissue injury and provide direct evidence that the hematopoietic compartment is not compromised. Finally, Sca1^+ mesenchymal interstitial cells and CD31^+ endothelial cells are also comparably present in mdx/mTR^Het and mdx/mTR^G2 muscle, suggesting that the severe phenotype is muscle specific and is not the result of functional defects in other cell types.

Amelioration of the Dystrophic Phenotype after Transplantation of WT MuSC

To test whether the dystrophic phenotype in mdx/mTR^G2 mice results from diminished MuSC reserve, we performed MuSC transplantation experiments into mdx/mTR^G2 dystrophic muscles. Freshly isolated MuSC, either WT or mdx/mTR^G2, were infected with a lentivirus expressing GFP, and 5000 cells were transplanted into irradiated tibialis anterior muscles of mdx/mTR^G2 mice (Figure 7D). The infection efficiency approximated 95% and was comparable among groups (p > 0.05; data not shown). Three weeks posttransplantation, WT MuSC efficiently engrafted into recipient muscles and contributed to an average of 299 ± 29 GFP^+ myofibers (Figures 7E and 7F and Figures S7F–S7J), whereas mdx/mTR^G2 MuSC contributed to substantially lower numbers of GFP^+ myofibers, 118 ± 17 (Figures 7E and 7F and Figures S7A–S7E). Measurements of fiber cross-sectional areas indicate that WT MuSC gave rise to larger myofibers compared to mdx/mTR^G2 (Figure 7G), indicating the ability to more robustly contribute to muscle upon transplantation. Further histological analysis revealed that the amount of inflammatory infiltration is substantially reduced in the muscle

region into which the WT MuSC were injected, compared to mdx/mTR^G2, as evidenced by the low numbers of CD45^+ hematopoietic cells and overall improvement in tissue architecture apparent in H&E sections (Figures S7K and S7L). The regenerative potential of transplanted MuSC from control mTR^G2 mice into mdx/mTR^G2 animals is similar to that observed with WT MuSC (data not shown). Together, these results provide strong evidence that the severe dystrophic phenotype observed in mdx/mTR^G2 mice results from loss of regenerative potential of endogenous MuSC. Although we cannot completely rule out the possibility of defects in other cell types or a direct effect on the myofiber itself as a potential contributing factor, these results demonstrate that progressive loss of MuSC reserve plays a major role in determining the severity of the dystrophic phenotype.

DISCUSSION

The absence of a mouse model for DMD that faithfully mimics key features of the human disease has limited our understanding of its pathophysiology and tests of potential therapies. A long-standing enigma has been why humans with a dystrophin mutation suffer from such severe muscle wasting, whereas mice with the same mutation do not. A major difference between humans and mice is the length of their telomeres, which are substantially shorter in humans. A reduction in telomere length in MuSC could severely limit the stem cell pool available for muscle repair over time. Here, we show that a new mouse model, mdx mice lacking telomerase activity (mdx/mTR), more closely recapitulates the DMD phenotype than mouse models described to date, as evidenced by characteristic severe progressive loss of muscle form and function.

We postulated that the severe muscle wasting phenotype observed in this mouse model is due to impaired function of the MuSC required for damage repair. We ruled out other possible stem cell etiologies such as premature MuSC differentiation or a reduction in MuSC numbers per myofiber at the time of disease onset. Instead, we determined both in vitro and in vivo that the MuSC from mdx/mTR^G2 mice suffer from severe defects in proliferation. In vivo, MuSC exhibited reduced division (BrdU labeling), smaller revertant clone sizes, inability to respond to injury, and markedly reduced engraftment upon transplantation into mice. In vitro, the proliferation defect was manifested by a marked reduction in the number of cells derived from single fibers. This proliferative defect correlated with an increase in signal-free chromosome ends and evidence of chromosome fusions normally not seen in low-turnover tissues such as muscle. Over time, a decrease in the number of MuSC per muscle fiber was observed. Presumably, the decrease in MuSC number in aged, dystrophic telomerase null mice ultimately reflects a failure of stem cell self-renewal. This reduction in MuSC number exacerbates the already impaired regeneration resulting from the reduced proliferative capacity of the remaining MuSC.

We reasoned that the replicative capacity of MuSC plays a role in murine muscle tissue homeostasis, overcoming the defect observed in human muscle lacking dystrophin. We confirmed this hypothesis here by coupling the absence of telomerase together with a constant pressure for muscle cell proliferation and regeneration caused by the mdx mutation. The result is
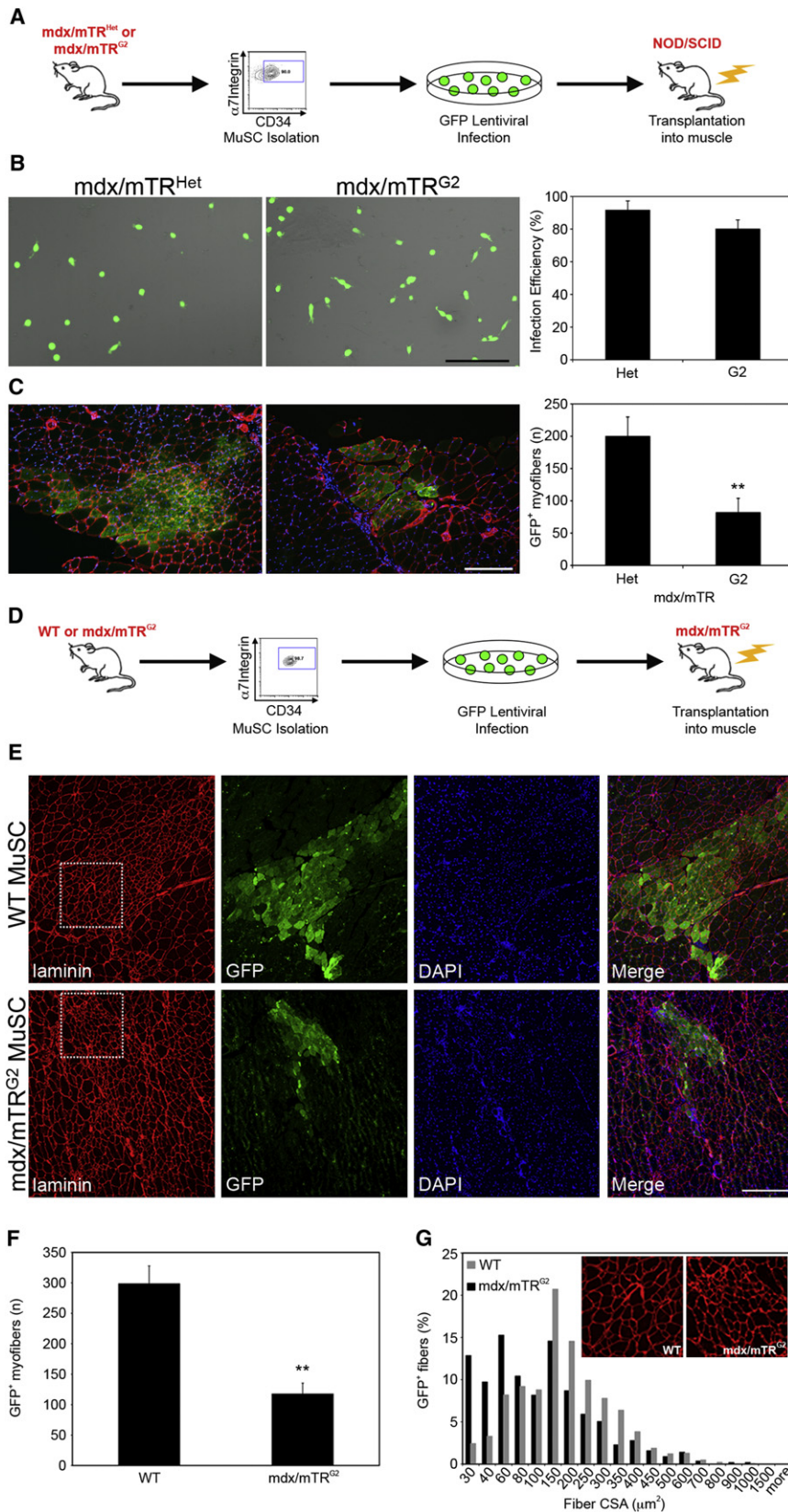
Figure 7. Muscle Stem Cells from mdx/mTR^{G2} Mice Exhibit Impaired Engraftment following Transplantation into Mouse Muscles

(A) Scheme of transplantation into NOD/SCID mice.

(B) Representative images of lentivirus-infected MuSC. Scale bar, 80 μm (left). Graph showing quantification of infection efficiency expressed as percentage of GFP$^+$ cells. Data are represented as average ± SEM (right). p > 0.05.

(C) Three weeks after transplantation, muscles were harvested, sectioned, and immunostained for GFP (green), laminin (red), and nuclear Hoechst (blue). Representative images of transplanted muscles. Scale bar, 120 μm (left). Graph showing total numbers of GFP$^+$ myofibers scored per muscle. Data are represented as average ± SEM. n ≥ 5; p < 0.01) (right).

(D) Scheme of transplantation into mdx/mTR^{G2} mice.

(E) Three weeks after transplantation, muscles were harvested, sectioned, and immunostained for GFP (green), laminin (red), and nuclear DAPI (blue). Representative images of transplanted muscles. Scale bar, 100 μm.

(F) Graph showing total numbers of GFP$^+$ myofibers per muscle. Data are represented as average ± SEM. n = 5; p < 0.05.

(G) Analysis of GFP$^+$ myofiber cross-sectional area after transplantation shows that WT MuSC give rise to larger myofibers compared to mdx/mTR^{G2} MuSC.

a mouse model, mdx/mTR^{G2}, that closely approximates the human disease. Muscles from DMD patients have been reported to have shorter telomeres than those of healthy individuals (Decary et al., 2000; Mouly et al., 2005). Similarly critical telomere shortening is evident here in cultured muscle progenitor cells isolated from mdx/mTR^{G2} mice with the muscular dystrophy phenotype. The generation of mouse models lacking telomerase activity, TERT and Terc knockout mice (Blasco et al., 1997; Liu et al., 2000), previously resulted in the demonstration that telomerase plays a crucial role in self-renewal of adult stem cells in high-turnover tissues such as blood, liver, skin, and testis (Allsopp et al., 2003; Lee et al., 1998). By contrast, skeletal muscle is a stable tissue, and a muscle phenotype in mice lacking TERT and Terc has never been reported. Even in the setting of continuous damage, the mdx model, only a mild muscle phenotype is apparent, and there is no evidence for telomere shortening in myoblasts of these mice. By contrast, we show here that murine MuSC progeny from mice lacking both dystrophin and telomerase exhibit a higher frequency of chromosomes with signal-free ends (chromosomes with critically shortened telomeres), compared to control mdx/mTR^{Het}, indicating that a persistent need for MuSC proliferation in vivo leads to telomere shortening, consequent senescence-like behavior, and tissue degeneration. These results provide definitive evidence that telomerase plays a crucial role in MuSC function in vivo. Although we cannot entirely rule out an effect of lack of telomerase on other cell types or mature myofibers, the findings highlight a cell-autonomous or intrinsic limitation as causal in hindering MuSC function.

Our findings of stem cell-autonomous defects are important to consider in light of recent studies that implicate a primary role of the environment in maintaining niche function and stem cell performance. Indeed, these studies show that stem cells from young and aged mice behave similarly when exposed to systemic factors from young mice via parabiosis (Brack et al., 2007; Conboy et al., 2005). Our results show that intrinsic characteristics such as telomere attrition are also critical to muscle regeneration and need to be taken into consideration when predicting the effects of modulating the environment on the function of human MuSC from aged or dystrophic muscles.

The etiology of the fibrosis observed in DMD remains unknown. Here, we observe that, when WT MuSC are transplanted into dystrophic mouse muscles, minimal fibrosis is observed, whereas fibrosis is extensive when proliferation-impaired mdx/mTR^{G2} MuSC are transplanted. These results are similar to those observed in chronic liver cirrhosis in which fibrosis and telomere shortening are correlated (Kitada et al., 1995; Rudolph et al., 2000; Wiemann et al., 2002). These findings suggest the intriguing possibility that, in chronically injured tissues, fibrosis is secondary to cell loss, not a primary competing process that antagonizes repair.

In summary, we provide evidence that telomere shortening is the result of continuous proliferation in degenerating dystrophic muscle and describe the generation of a new DMD mouse model that more faithfully recapitulates the disease progression in humans. This model will prove useful for elucidating the pathophysiology of DMD and for testing potential therapeutic approaches for this and other muscle wasting diseases, which

has been hindered by the mild phenotypes that are typical of currently available mouse models. Our results indicate that DMD, a muscle degenerative disease, is the result of a multifactorial process, due to both a structural defect of the tissue and progressive exhaustion of its regenerative potential. Therapeutic interventions should consider both telomere length as well as myogenic potential of the regenerative cell source in order to overcome previous limitations (Gussoni et al., 1992). Together, these data document the importance of telomerase in muscle homeostasis and provide the first direct experimental evidence that DMD progression, although initiated and driven by dystrophin deficiency, is ultimately a stem cell disease.

EXPERIMENTAL PROCEDURES

Animals
All protocols were approved by the Stanford University Administrative Panel on Laboratory Animal Care. C57Bl6 mdx mice (purchased from Jackson Laboratories) and C57Bl6 mTR^{Het} mice (a kind gift from Ron DePinho) were used to generate the double-mutant animals. The NOD/SCID-immunodeficient mice were purchased from the Jackson Laboratories.

Single-Fiber Isolation and Satellite Cell Staining
Single myofibers were isolated from tibialis anterior muscles for all genotypes as previously described (Collins et al., 2005). See Extended Experimental Procedures for a detailed description of the procedure.

Force Measurements
Eight-week-old mice were anesthetized and force measurements of lateral gastrocnemius muscle were performed in vivo on anesthetized animals in accordance with Stanford guidelines. See Extended Experimental Procedures for a detailed description of the procedure.

Treadmill Test
The treadmill test was performed using the Exer3/6 (Columbus Instruments). Mice were acclimated to treadmill running for three times (every other day) before the test was performed. Mice ran on the treadmill at 20 degrees downhill, starting at a speed of 10 meters/min. After 3 min, the speed was increased 1 meter/min to a final speed of 20 meter/min. Exhaustion was defined as the inability of the animal to remain on the treadmill despite electrical prodding.

SPECT/CT Animal Imaging
Anesthetized (3% isofluorane) animals were placed into SPECT-CT scanner (Gamma-Medica-Ideas Pre-clinical Imaging) with high-energy resolution CZT detectors and multipin-hole collimators. See Extended Experimental Procedures for a detailed description of the procedure.

Irradiation, Cell Transplantation, and Notexin Damage
NOD/SCID and mdx/mTR^{G2} mice were anesthetized and shielded in a lead-jig so that only the legs were exposed to the radiation source. A single dose of 18Gy was administered to the legs, and cell transplantation was performed on the same day. Lentivirus-infected MuSC were resuspended in PBS, and a 10 μl of cell suspension was injected intramuscularly into the tibialis anterior (TA) muscles of recipient mice. For local tissue injury, mice were anesthetized with isofluorane, and a single 10 μl injection of notexin (10 μg/ml, Latoxan, France) was injected into the TAs of recipient mice.

In Vivo BrdU Labeling
Mice were anesthetized with isofluorane and weighed, and a single dose of BrdU in PBS was delivered intraperitoneally (100 mg/Kg body weight). Twenty-four hours later, mice were sacrificed and MuSC isolated, as previously described (Sacco et al., 2008). After FACS enrichment, MuSC were cytospun onto slides, fixed, and stained using a BrdU labeling and detection kit (Roche).

Telomere Fluorescence In Situ Hybridization

For telomere measurements, primary myoblasts were isolated as previously described (Rando and Blau, 1994) and maintained in culture in F10/DMEM + 15%FBS + βFGF media. See Extended Experimental Procedures for a detailed description of the procedure.

Lentiviral Infection

The five plasmid system and infection protocol used here has been previously described (Westerman et al., 2007). See Extended Experimental Procedures for a detailed description of the procedure.

Cell Culture

Cells were isolated from muscle tissue by enzymatic dissociation as described above. Cells were plated on dishes coated with laminin (Roche) in F10/DMEM (50/50) + 15%FBS + 2.5ng/ml βFGF (GM) for proliferation and in DMEM + 2% horse serum (DM) for differentiation.

Image Acquisition of Immunofluorescence and Histology

Images of muscle transverse sections were acquired using an epifluorescence microscope (Axioplan2, Carl Zeiss MicroImaging, Inc.), Fluar 20X/0.75 objective lens, and a digital camera (ORCA-ER C4742-95; Hamamatsu Photonics). The software used for acquisition was OpenLab 4.0.2 (Improvision). Images of cell cultures were acquired using a laser-scanning confocal microscope (LSM510, Carl Zeiss MicroImaging, Inc.) using Plan NeoFluar 10×/0.3 and 20×/0.75 objective lens and maximum optical sections with the LSM software. All images were composed and edited in Photoshop 7.0 (Adobe). Background was reduced using brightness and contrast adjustments, and color balance was performed to enhance colors. All of the modifications were applied to the whole image using Photoshop 7.0 (Adobe).

Statistical Analysis

Data are presented as mean ± SEM. Comparisons between groups used the Student's t test assuming two-tailed distributions, with an alpha level of 0.01–0.05.

SUPPLEMENTAL INFORMATION

Supplemental Information includes Extended Experimental Procedures and seven figures and can be found with this article online at doi:10.1016/j.cell. 2010.11.039.

REFERENCES

Aikata, H., Takaishi, H., Kawakami, Y., Takahashi, S., Kitamoto, M., Nakanishi, T., Nakamura, Y., Shimamoto, F., Kajiyama, G., and Ide, T. (2000). Telomere reduction in human liver tissues with age and chronic inflammation. Exp. Cell Res. 256, 578–582.

Allsopp, R.C., Morin, G.B., DePinho, R., Harley, C.B., and Weissman, I.L. (2003). Telomerase is required to slow telomere shortening and extend replicative lifespan of HSCs during serial transplantation. Blood 102, 517–520.

Artandi, S.E. (2006). Telomeres, telomerase, and human disease. N. Engl. J. Med. 355, 1195–1197.

Blaauw, B., Mammucari, C., Toniolo, L., Agatea, L., Abraham, R., Sandri, M., Reggiani, C., and Schiaffino, S. (2008). Akt activation prevents the force drop induced by eccentric contractions in dystrophin-deficient skeletal muscle. Hum. Mol. Genet. 17, 3686–3696.

Blasco, M.A., Lee, H.W., Hande, M.P., Samper, E., Lansdorp, P.M., DePinho, R.A., and Greider, C.W. (1997). Telomere shortening and tumor formation by mouse cells lacking telomerase RNA. Cell 91, 25–34.

Blau, H.M., Webster, C., and Pavlath, G.K. (1983). Defective myoblasts identified in Duchenne muscular dystrophy. Proc. Natl. Acad. Sci. USA 80, 4856–4860.

Bockhold, K.J., Rosenblatt, J.D., and Partridge, T.A. (1998). Aging normal and dystrophic mouse muscle: analysis of myogenicity in cultures of living single fibers. Muscle Nerve 21, 173–183.

Brack, A.S., Conboy, M.J., Roy, S., Lee, M., Kuo, C.J., Keller, C., and Rando, T.A. (2007). Increased Wnt signaling during aging alters muscle stem cell fate and increases fibrosis. Science 317, 807–810.

Bulfield, G., Siller, W.G., Wight, P.A., and Moore, K.J. (1984). X chromosome-linked muscular dystrophy (mdx) in the mouse. Proc. Natl. Acad. Sci. USA 81, 1189–1192.

Cerletti, M., Jurga, S., Witczak, C.A., Hirshman, M.F., Shadrach, J.L., Goodyear, L.J., and Wagers, A.J. (2008). Highly efficient, functional engraftment of skeletal muscle stem cells in dystrophic muscles. Cell 134, 37–47.

Chang, S., Multani, A.S., Cabrera, N.G., Naylor, M.L., Laud, P., Lombard, D., Pathak, S., Guarente, L., and DePinho, R.A. (2004). Essential role of limiting telomeres in the pathogenesis of Werner syndrome. Nat. Genet. 36, 877–882.

Collins, C.A., Olsen, I., Zammit, P.S., Heslop, L., Petrie, A., Partridge, T.A., and Morgan, J.E. (2005). Stem cell function, self-renewal, and behavioral heterogeneity of cells from the adult muscle satellite cell niche. Cell 122, 289–301.

Conboy, I.M., Conboy, M.J., Wagers, A.J., Girma, E.R., Weissman, I.L., and Rando, T.A. (2005). Rejuvenation of aged progenitor cells by exposure to a young systemic environment. Nature 433, 760–764.

Cornelison, D.D., Wilcox-Adelman, S.A., Goetinck, P.F., Rauvala, H., Rapraeger, A.C., and Olwin, B.B. (2004). Essential and separable roles for Syndecan-3 and Syndecan-4 in skeletal muscle development and regeneration. Genes Dev. 18, 2231–2236.

Decary, S., Mouly, V., Hamida, C.B., Sautet, A., Barbet, J.P., and Butler-Browne, G.S. (1997). Replicative potential and telomere length in human skeletal muscle: implications for satellite cell-mediated gene therapy. Hum. Gene Ther. 8, 1429–1438.

Decary, S., Hamida, C.B., Mouly, V., Barbet, J.P., Hentati, F., and Butler-Browne, G.S. (2000). Shorter telomeres in dystrophic muscle consistent with extensive regeneration in young children. Neuromuscul. Disord. 10, 113–120.

DiMario, J.X., Uzman, A., and Strohman, R.C. (1991). Fiber regeneration is not persistent in dystrophic (MDX) mouse skeletal muscle. Dev. Biol. 148, 314–321.

Durbeej, M., and Campbell, K.P. (2002). Muscular dystrophies involving the dystrophin-glycoprotein complex: an overview of current mouse models. Curr. Opin. Genet. Dev. 12, 349–361.

Emery, A.E. (2002). The muscular dystrophies. Lancet 359, 687–695.

Friedrich, U., Griese, E., Schwab, M., Fritz, P., Thon, K., and Klotz, U. (2000). Telomere length in different tissues of elderly patients. Mech. Ageing Dev. 119, 89–99.

Greider, C.W., and Blackburn, E.H. (1985). Identification of a specific telomere terminal transferase activity in Tetrahymena extracts. Cell 43, 405–413.

Gussoni, E., Pavlath, G.K., Lanctot, A.M., Sharma, K., Miller, R.G., Steinman, L., and Blau, H.M. (1992). Normal dystrophin transcripts detected in DMD patients after myoblast transplantation. Nature *356*, 435–438.

Harris, J.B., and MacDonell, C.A. (1981). Phospholipase A2 activity of notexin and its role in muscle damage. Toxicon *19*, 419–430.

Hemann, M.T., Rudolph, K.L., Strong, M.A., DePinho, R.A., Chin, L., and Greider, C.W. (2001). Telomere dysfunction triggers developmentally regulated germ cell apoptosis. Mol. Biol. Cell *12*, 2023–2030.

Herrera, E., Samper, E., and Blasco, M.A. (1999). Telomere shortening in mTR-/- embryos is associated with failure to close the neural tube. EMBO J. *18*, 1172–1181.

Hoffman, E.P., Brown, R.H., Jr., and Kunkel, L.M. (1987). Dystrophin: the protein product of the Duchenne muscular dystrophy locus. Cell *51*, 919–928.

Hoffman, E.P., Morgan, J.E., Watkins, S.C., and Partridge, T.A. (1990). Somatic reversion/suppression of the mouse mdx phenotype in vivo. J. Neurol. Sci. *99*, 9–25.

Im, W.B., Phelps, S.F., Copen, E.H., Adams, E.G., Slightom, J.L., and Chamberlain, J.S. (1996). Differential expression of dystrophin isoforms in strains of mdx mice with different mutations. Hum. Mol. Genet. *5*, 1149–1153.

Kipling, D., and Cooke, H.J. (1990). Hypervariable ultra-long telomeres in mice. Nature *347*, 400–402.

Kitada, T., Seki, S., Kawakita, N., Kuroki, T., and Monna, T. (1995). Telomere shortening in chronic liver diseases. Biochem. Biophys. Res. Commun. *211*, 33–39.

Kuang, S., Kuroda, K., Le Grand, F., and Rudnicki, M.A. (2007). Asymmetric self-renewal and commitment of satellite stem cells in muscle. Cell *129*, 999–1010.

Lee, H.W., Blasco, M.A., Gottlieb, G.J., Horner, J.W., 2nd, Greider, C.W., and DePinho, R.A. (1998). Essential role of mouse telomerase in highly proliferative organs. Nature *392*, 569–574.

Lindsey, J., McGill, N.I., Lindsey, L.A., Green, D.K., and Cooke, H.J. (1991). In vivo loss of telomeric repeats with age in humans. Mutat. Res. *256*, 45–48.

Liu, Y., Snow, B.E., Hande, M.P., Yeung, D., Erdmann, N.J., Wakeham, A., Itie, A., Siderovski, D.P., Lansdorp, P.M., Robinson, M.O., and Harrington, L. (2000). The telomerase reverse transcriptase is limiting and necessary for telomerase function in vivo. Curr. Biol. *10*, 1459–1462.

McDonald, C.M., Abresch, R.T., Carter, G.T., Fowler, W.M., Jr., Johnson, E.R., Kilmer, D.D., and Sigford, B.J. (1995). Profiles of neuromuscular diseases. Duchenne muscular dystrophy. Am. J. Phys. Med. Rehabil. *74*(5, Suppl), S70–S92.

Montarras, D., Morgan, J., Collins, C., Relaix, F., Zaffran, S., Cumano, A., Partridge, T., and Buckingham, M. (2005). Direct isolation of satellite cells for skeletal muscle regeneration. Science *309*, 2064–2067.

Mouly, V., Aamiri, A., Bigot, A., Cooper, R.N., Di Donna, S., Furling, D., Gidaro, T., Jacquemin, V., Mamchaoui, K., Negroni, E., et al. (2005). The mitotic clock in skeletal muscle regeneration, disease and cell mediated gene therapy. Acta Physiol. Scand. *184*, 3–15.

Oda, T., Shimizu, N., Yonenobu, K., Ono, K., Nabeshima, T., and Kyoh, S. (1993). Longitudinal study of spinal deformity in Duchenne muscular dystrophy. J. Pediatr. Orthop. *13*, 478–488.

Palm, W., and de Lange, T. (2008). How shelterin protects mammalian telomeres. Annu. Rev. Genet. *42*, 301–334.

Petrof, B.J., Shrager, J.B., Stedman, H.H., Kelly, A.M., and Sweeney, H.L. (1993). Dystrophin protects the sarcolemma from stresses developed during muscle contraction. Proc. Natl. Acad. Sci. USA *90*, 3710–3714.

Rando, T.A., and Blau, H.M. (1994). Primary mouse myoblast purification, characterization, and transplantation for cell-mediated gene therapy. J. Cell Biol. *125*, 1275–1287.

Renault, V., Rolland, E., Thornell, L.E., Mouly, V., and Butler-Browne, G. (2002). Distribution of satellite cells in the human vastus lateralis muscle during aging. Exp. Gerontol. *37*, 1513–1514.

Rodier, F., Kim, S.H., Nijjar, T., Yaswen, P., and Campisi, J. (2005). Cancer and aging: the importance of telomeres in genome maintenance. Int. J. Biochem. Cell Biol. *37*, 977–990.

Rudolph, K.L., Chang, S., Lee, H.W., Blasco, M., Gottlieb, G.J., Greider, C., and DePinho, R.A. (1999). Longevity, stress response, and cancer in aging telomerase-deficient mice. Cell *96*, 701–712.

Rudolph, K.L., Chang, S., Millard, M., Schreiber-Agus, N., and DePinho, R.A. (2000). Inhibition of experimental liver cirrhosis in mice by telomerase gene delivery. Science *287*, 1253–1258.

Ryder-Cook, A.S., Sicinski, P., Thomas, K., Davies, K.E., Worton, R.G., Barnard, E.A., Darlison, M.G., and Barnard, P.J. (1988). Localization of the mdx mutation within the mouse dystrophin gene. EMBO J. *7*, 3017–3021.

Sacco, A., Doyonnas, R., Kraft, P., Vitorovic, S., and Blau, H.M. (2008). Self-renewal and expansion of single transplanted muscle stem cells. Nature *456*, 502–506.

Sherr, C.J., and DePinho, R.A. (2000). Cellular senescence: mitotic clock or culture shock? Cell *102*, 407–410.

Straub, V., Rafael, J.A., Chamberlain, J.S., and Campbell, K.P. (1997). Animal models for muscular dystrophy show different patterns of sarcolemmal disruption. J. Cell Biol. *139*, 375–385.

Takubo, K., Nakamura, K., Izumiyama, N., Furugori, E., Sawabe, M., Arai, T., Esaki, Y., Mafune, K., Kammori, M., Fujiwara, M., et al. (2000). Telomere shortening with aging in human liver. J. Gerontol. A Biol. Sci. Med. Sci. *55*, B533–B536.

Vaziri, H., Schächter, F., Uchida, I., Wei, L., Zhu, X., Effros, R., Cohen, D., and Harley, C.B. (1993). Loss of telomeric DNA during aging of normal and trisomy 21 human lymphocytes. Am. J. Hum. Genet. *52*, 661–667.

Webster, C., and Blau, H.M. (1990). Accelerated age-related decline in replicative life-span of Duchenne muscular dystrophy myoblasts: implications for cell and gene therapy. Somat. Cell Mol. Genet. *16*, 557–565.

Webster, C., Filippi, G., Rinaldi, A., Mastropaolo, C., Tondi, M., Siniscalco, M., and Blau, H.M. (1986). The myoblast defect identified in Duchenne muscular dystrophy is not a primary expression of the DMD mutation. Clonal analysis of myoblasts from five double heterozygotes for two X-linked loci: DMD and G6PD. Hum. Genet. *74*, 74–80.

Westerman, K.A., Ao, Z., Cohen, E.A., and Leboulch, P. (2007). Design of a trans protease lentiviral packaging system that produces high titer virus. Retrovirology *4*, 96.

Wiemann, S.U., Satyanarayana, A., Tsahuridu, M., Tillmann, H.L., Zender, L., Klempnauer, J., Flemming, P., Franco, S., Blasco, M.A., Manns, M.P., and Rudolph, K.L. (2002). Hepatocyte telomere shortening and senescence are general markers of human liver cirrhosis. FASEB J. *16*, 935–942.

Wilkins, K.E., and Gibson, D.A. (1976). The patterns of spinal deformity in Duchenne muscular dystrophy. J. Bone Joint Surg. Am. *58*, 24–32.

Wong, K.K., Maser, R.S., Bachoo, R.M., Menon, J., Carrasco, D.R., Gu, Y., Alt, F.W., and DePinho, R.A. (2003). Telomere dysfunction and Atm deficiency compromises organ homeostasis and accelerates ageing. Nature *421*, 643–648.

Zatz, M., Rapaport, D., Vainzof, M., Passos-Bueno, M.R., Bortolini, E.R., Pavanello, Rde.C., and Peres, C.A. (1991). Serum creatine-kinase (CK) and pyruvate-kinase (PK) activities in Duchenne (DMD) as compared with Becker (BMD) muscular dystrophy. J. Neurol. Sci. *102*, 190–196.

Supplemental Information

EXTENDED EXPERIMENTAL PROCEDURES

Muscle Stem Cell Isolation

Tibialis anterior muscles of mice were subjected to enzymatic dissociation (first collagenase 0.2%, then dispase 0.04U/ml, SIGMA) for 90 min, after which nonmuscle tissue was gently removed under a dissection microscope. The cell suspension was filtered through a 70 μm Nylon filter (Falcon) and incubated with the following biotinylated antibodies: CD45, CD11b, CD31 and Sca1 (BD Bioscience). Streptavidin beads (Miltenyi Biotech) were then added to the cells together with the following antibodies: α7integrin-Phycoerythrin (PE)(kind gift from Fabio Rossi, BRC, University of British Columbia, Vancouver, Canada) and CD34-Alexa637 (eBioscience), after which magnetic depletion of biotin-positive cells was performed. The (CD45$^-$CD11b$^-$CD31$^-$Sca1$^-$) CD34$^+\alpha$7integrin$^+$ population was then fractionated twice by flow-cytometry (DIVA-Van, Becton Dickinson). Primary myoblasts were isolated as previously described (Rando and Blau, 1994).

Single-Fiber Isolation

Muscles were explanted and subjected to enzymatic dissociation. After 90 min, fibers were gently released from the tissue under a dissecting scope and separated from tissue debris. Fibers were immediately fixed in paraformaldehyde 1.5% for 20 min and washed in PBS. For immunostaining, fibers were blocked in 20% goat serum + 0.5% Triton + AntiFcIgG Fab Fragment (SIGMA) in PBS for 1 hr. Primary antibody Pax7 (DHSB) was incubated over night at 4C. After PBS washes, fibers were incubated with Alexa488 anti mouse antibody for 1 hr in the dark. Fibers were washed in PBS overnight, and mounted with Fluoromount onto slides for microscopic analysis.

SPECT/CT Animal Imaging

512 images per animal were acquired using GMI software at 1.25 magnification (FOV 94.72 mm and voxel size 0.185 mm) and FLEX SPECT-Version 1.0.6 was used for image reconstitution. Files were converted into dcim using GEHC Microview and further analyzed in OsiriX.

Lentiviral Infection

The bottom of a 48-well plate was coated with 100 ul of retronectin/PBS (final concentration of 20ug/ml). After 2 hr, the retronectin solution was removed, and 200 ul of 2% BSA was added for 30 min at RT. The wells were then washed with Hank's balanced salt solution containing 2.5% of 1M HEPES. In the meantime, the desired amount of virus was incubated with protamine sulfate. Cells and virus suspension were plated in the 48-well plate and incubated overnight at 37°C. The next day, cells were collected, counted, and injected i.m. into tibialis anterior muscles of irradiated NOD/SCID recipient mice.

Force Measurements

Force measurements were performed on gastrocnemius muscles in situ in anesthetized mice, as previously described (Blaauw et al., 2008). The hindlimb was shaved and fixed to a frame in order to immobilize it without compromising the blood supply to the leg. The animal was warmed on an isothermal pad and by heat lamp. A small incision was placed in the skin directly above the lateral gastrocnemius. Single stranded stainless steel hook electrodes (50 μm, bared 1mm from tip) were inserted in the muscle by 30-gauge hypodermic needle. We used a differential electrode arrangement with one EMG electrode placed in the belly of the muscle, one near where the muscle inserts into the tendon, and one adjacent to the site of stimulation, and recorded at 100 kHz. The Achilles tendon of the animal was then cut from the calcaneous, leaving the distal end of the calcaneous attached to the tendon. The Achilles tendon was then attached to a force transducer (Aurora Scientific, 300C-LR) by a thin metal hook. All tendons from muscles not being measured were cut free from the Achilles tendon, leaving only the lateral gastrocnemius attached. The muscles and tendons were kept moist by periodic wetting with Ringer's solution. Next, a small incision was placed in the skin parallel and inferior to the midlateral femur. Then a deeper cut was made in the fasciae of the hamstrings to expose the sciatic nerve. The sciatic nerve was then gently freed from the surrounding tissue so that a cuff could be placed around it, using small electrically isolated instruments. Then a bipolar electrical stimulation cuff was placed around the sciatic nerve. The sciatic nerve was moistened periodically with Ringer's solution, but no fluid collection around the nerve was allowed. In all experiments we used 0.1 ms pulses at predetermined supra-maximal stimulation intensity. During twitch trials, the sciatic nerve was stimulated at 1 Hz for 5 s. During tetanic trials, the sciatic nerve was stimulated at 100Hz, which is approximately 0.75 times the average relaxation time for a single twitch, for 0.3 s. Muscle force, EMG and synchronization pulses were recorded at 100 kHz for 2 s immediately prior to the stimulation and 3 s after the last stimulation. After completion of in vivo experiments the animals were sacrificed by cervical dislocation. All data were analyzed in Matlab (Mathworks).

Grid Test

Mice were lifted by their tails and placed on a horizontal grid as previously described (Tillerson and Miller, 2003). The grid was then inverted and the mice were hanging upside down by their paws and the length of the time staying on the grid was measured. Each animal was given 1 hr to rest and then tested for another 2 times (total tests per animal = 3).

Telomeric Fluorescence In Situ Hybridization (Telomere FISH)

All myoblast populations isolated from mice of different genotypes were analyzed at passage 8. Myoblasts were treated with 0.1 μg/ml Colcemid (Invitrogen) for 3 hr, trypsinized and swelled in 0.56% KCl at 37°C for 15 min, fixed in 3:1 methanol/glacial acetic acid at 4°C, and dropped on slides to prepare metaphase chromosomal spreads. Slides were then air-dried overnight, fixed with 4% formaldehyde in PBS for 2 min, treated with 1mg/ml pepsin (Sigma) in 0.01N HCl pH 2.0 at 37°C for 10 min, re-fixed with 4% formaldehyde, dehydrated with ethanol series, and air-dried again prior to hybridization. Chromosomal DNA was hybridized with a Cy3-conjugated $(CCCTAA)_3$ peptide-nucleic acid probe (Applied Biosystems) by using a hybridization mixture containing 70% deionized formamide, 0.25% blocking reagent (FP1020, Perkin Elmer), 5 mM Tris-Cl pH 7.4, 0.5 μg/ml PNA Cy3-telomere probe, 4.1 mM NaH_2PO_4, 0.45 mM citric acid, 1 mM $MgCl_2$. After heat denaturing DNA on slides at 80°C for 3 min, hybridization was carried out at room temperature for 3 hr. Slides were then washed with buffer I (10 mM Tris-HCl pH 7.4, 70% deionized formamide, 0.1% BSA) and buffer II (0.1 M Tris-Cl pH 7.4, 0.15 M NaCl, 0.1% Tween 20), dehydrated with ethanol series, air-dried, and mounted with Vectashield (Vector labs) with DAPI (0.2 μg/ml). Cy3 and DAPI images were taken by using 63X objective on Leica DM5000B microscope and Leica DFC 360FX CCD camera. At least 600 chromosomes (>2,400 telomeres) per genotype with two or three replicates were analyzed to determine the presence of non-detectable telomere signals (signal-free ends) at chromosomal ends by Cy3 photos taken with maximum exposure settings.

SUPPLEMENTAL REFERENCES

Blaauw, B., Mammucari, C., Toniolo, L., Agatea, L., Abraham, R., Sandri, M., Reggiani, C., and Schiaffino, S. (2008). Akt activation prevents the force drop induced by eccentric contractions in dystrophin-deficient skeletal muscle. Hum. Mol. Genet. 17, 3686–3696.

Lee, H.W., Blasco, M.A., Gottlieb, G.J., Horner, J.W., II, Greider, C.W., and DePinho, R.A. (1998). Essential role of mouse telomerase in highly proliferative organs. Nature 392, 569–574.

Rando, T.A., and Blau, H.M. (1994). Primary mouse myoblast purification, characterization, and transplantation for cell-mediated gene therapy. J. Cell Biol. 125, 1275–1287.

Tillerson, J.L., and Miller, G.W. (2003). Grid performance test to measure behavioral impairment in the MPTP-treated-mouse model of parkinsonism. J. Neurosci. Methods 123, 189–200.
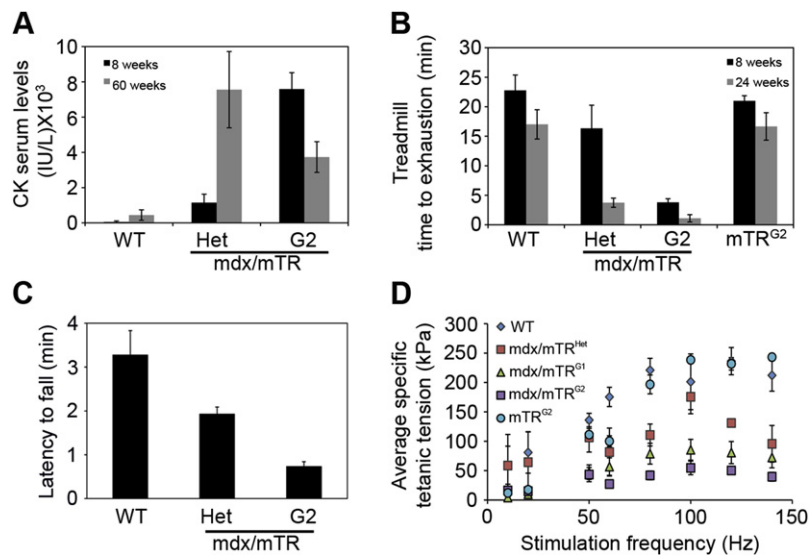
Figure S1. Muscle Performance Progressively Deteriorates in mdx/mTR^{G2} Mice with Age, Related to Figure 1

(A) Serum creatine kinase (CK) levels, a strong indicator of skeletal muscle damage, in 8 and 60 weeks old males of the various genotypes. Data are represented as average ± s.e.m. (n ≥ 5, p > 0.05).

(B) 8 and 24 weeks old mice were subjected to the treadmill test and their performance was measured as time to exhaustion. Exhaustion was defined as the inability of the animal to remain on the treadmill despite electrical prodding. As shown, muscle performance of mdx/mTR^{G2} mice severely worsens with age (n ≥ 5, p < 0.03).

(C) 8 weeks old mice were subjected to the grid test, and their performance was measured as time they were able to hold onto it until falling. As shown, mdx/mTR^{G2} mice were substantially impaired in this test (n = 3; p < 0.03).

(D) Lateral gastrocnemius muscles of 8 weeks old mice of the indicated genotypes were stimulated through the sciatic nerve at different frequencies and the generated force was recorded. Results are shown as average ± s.e.m (n = 3; p < 0.03).
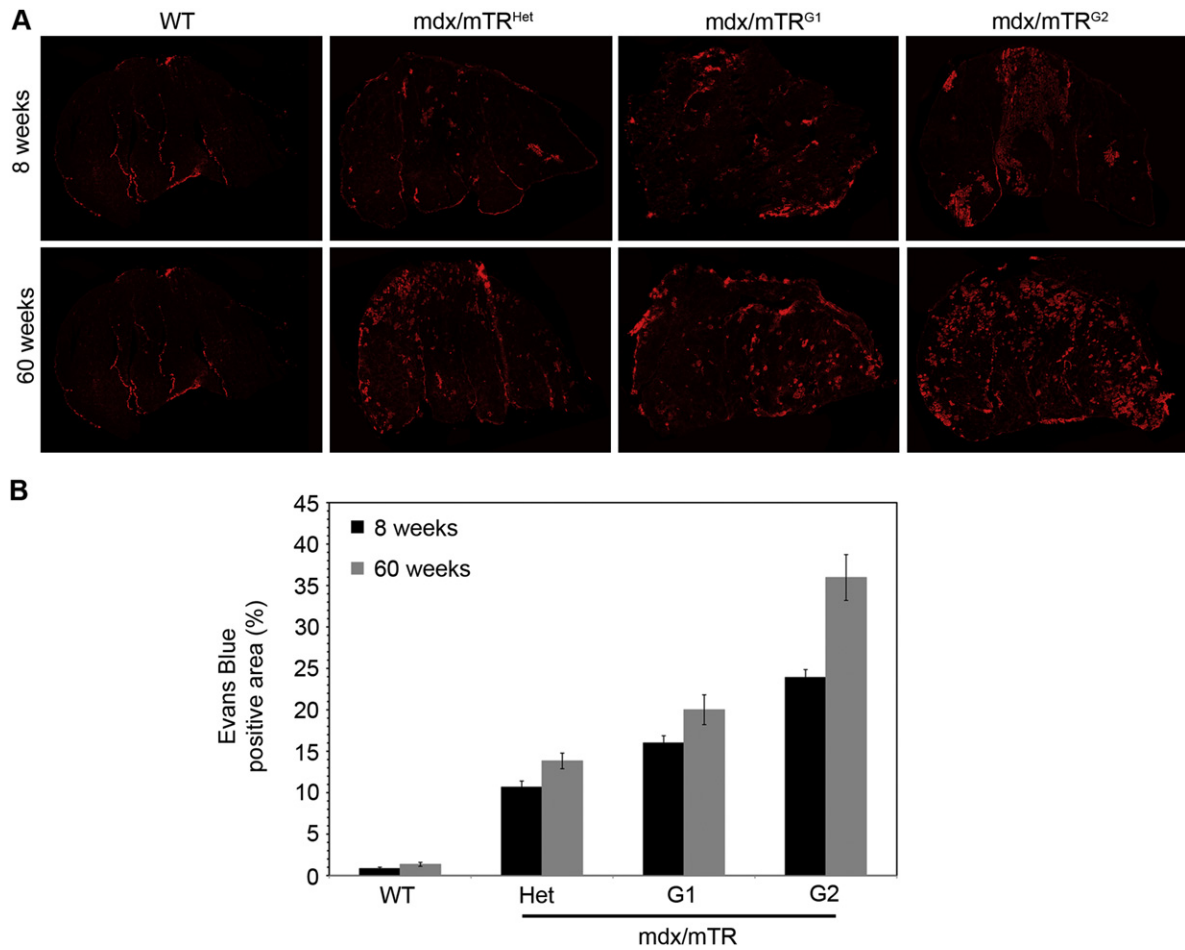
Figure S2. Membrane Permeability Is Increased in mdx/mTR^G2 Gastrocnemius Muscles and Deteriorates with Age, Related to Figure 2

(A) Images of Evans blue dye incorporation in gastrocnemius muscles from 8 and 60 weeks old animals of the indicated genotypes.

(B) Quantification of Evans blue dye incorporation in gastrocnemius muscles. Results are shown as average ± s.e.m (n = 3, p < 0.05).
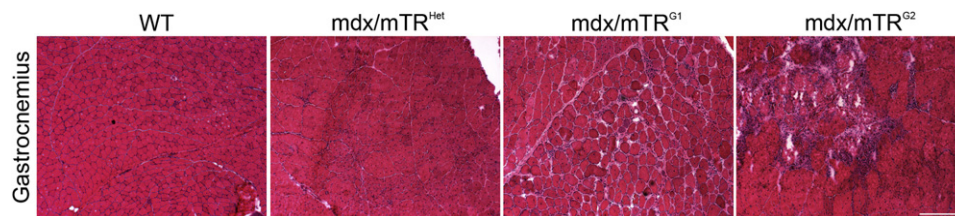
Figure S3. Muscle Histology of mdx/mTR^{G2} Muscles Deteriorates with Age, Related to Figure 3

Hematoxylin/eosin staining of gastrocnemius muscle from mice at 60 weeks of age revealed progression of the disease, with large areas of tissue damage. Scale bar, 200 μm.
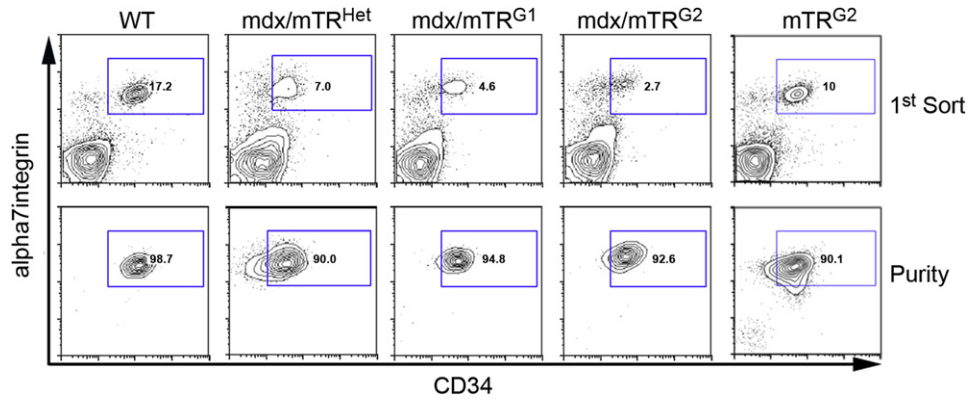
**Figure S4. Isolation of MuSCs by FACS, Related to Figure 4**

Tibialis anterior muscles from 8 week old mice were harvested, digested with collagenase and dispase, and stained for surface markers as described in detail in Extended Experimental Procedures. Briefly, nonmuscle cells were eliminated from cell samples by magnetic depletion and muscle stem cells were enriched using α7integrin and CD34, as previously described (Sacco et al., 2008), achieving a purity for all genotypes of > 90%.
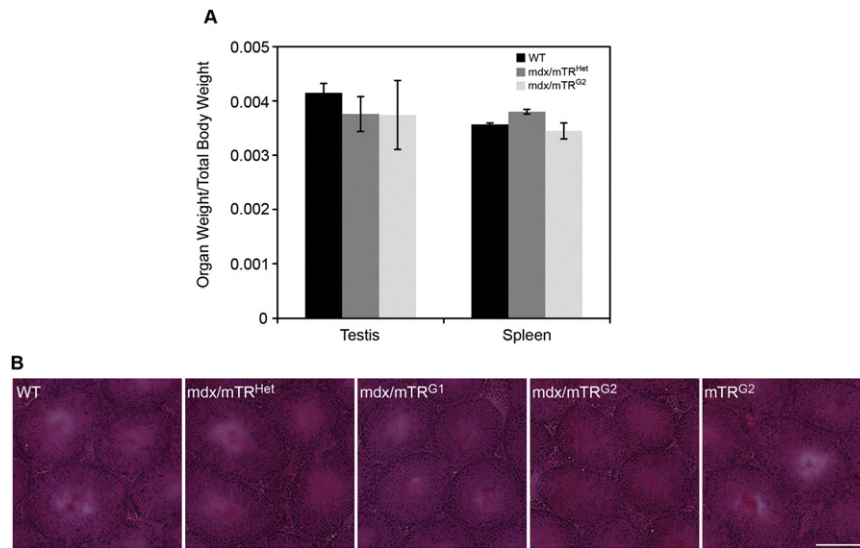
Figure S5. Highly Proliferative Tissues, Testis and Spleen, Do Not Exhibit Signs of Atrophy in mdx/mTR^{G2} Mice, Related to Figure 5

(A) Tissues were harvested from mice at 8 weeks of age and weighted. Data are represented as the weight of the tissue divided by the weight of the whole mouse, a standard control for telomere shortening (Lee et al., 1998). Highly proliferative organs with substantial cell turnover, such as testis and spleen, do not display significant differences in weight at G2. Data are represented as average ± s.e.m. (n = 3, p > 0.05).

(B) Testis was isolated from 8 week old mice of each genotype, sectioned and stained with hematoxylin-eosin, a standard control for telomere deficiency (Lee et al., 1998). The morphology of testes from mdx/mTR^{G2} mice was indistinguishable from all other genotypes, indicating that critical telomere shortening in high proliferative organs did not take place in the generations analyzed. Scale Bars, 100 μm.
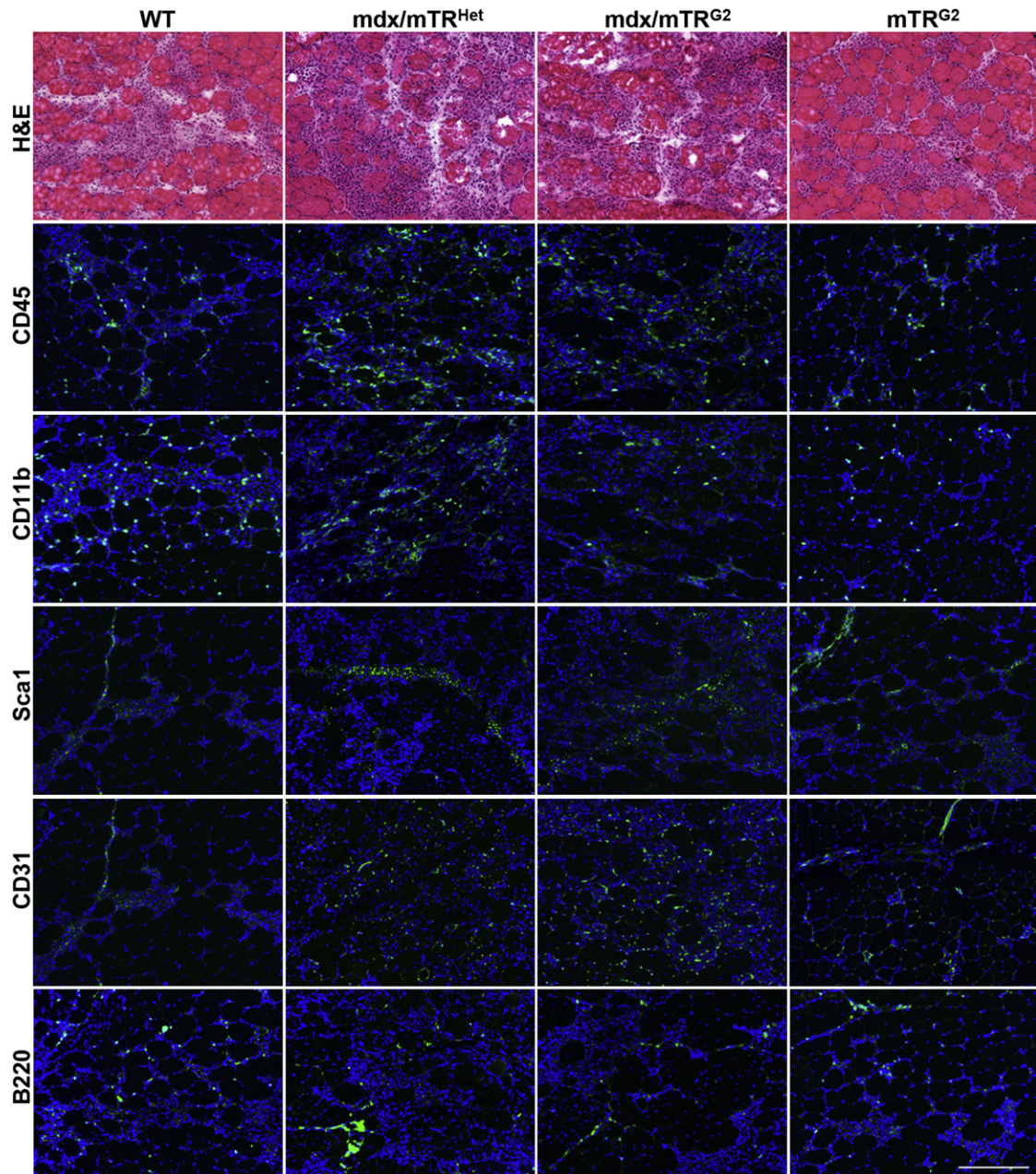
Figure S6. Nonmuscle Cell Types Are Not Affected in mdx/mTR^{G2} Mice, Related to Figure 6
Tibialis anterior muscles from 8 week old mice were damaged by notexin injection, and tissues were harvested at day 3 after injury and stained for hematoxylin/eosin (top panels) or immunostained for the indicated non-muscle markers (green) and nuclei (DAPI, blue) (bottom panels). Scale bar, 60 μm.
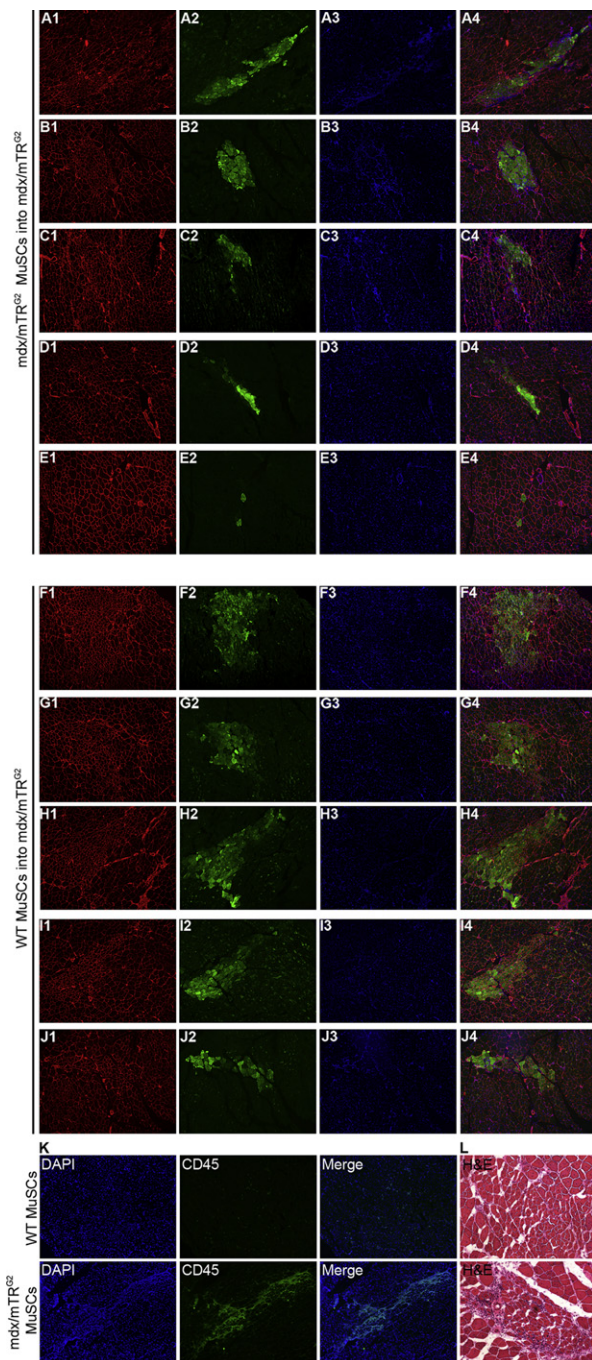
Figure S7. Transplantation of WT MuSCs Ameliorates the Muscle Histology of mdx/mTR^{G2} Mice, Related to Figure 7

(A–E) Immunofluorescence images of all irradiated 8 week old mdx/mTR^{G2} muscles transplanted with mdx/mTR^{G2} MuSCs, described in Figure 7 (red = laminin, green = GFP, blue = DAPI).

(F–J) Immunofluorescence images of all irradiated 8 week old irradiated mdx/mTR^{G2} muscles transplanted with WT MuSCs, described in Figure 7 (red = laminin, green = GFP, blue = DAPI).

(K) Immunofluorescence for CD45 (green) on irradiated 8 week old irradiated mdx/mTR^{G2} muscles transplanted with either WT or mdx/mTR^{G2} MuSCs (blue = DAPI).

(L) Hematoxylin/eosin staining of irradiated 8 week old irradiated mdx/mTR^{G2} muscles transplanted with either WT (top panel) or mdx/mTR^{G2} MuSCs (bottom panel). Scale Bar for all images, 100 μm.